MOLECULAR ASSEMBLY OF HYALURONIC ACID NANOPARTICLES FOR DRUG DELIVERY BY MOLECULAR DYNAMICS SIMULATION

Mr. Pisit Lerttanakij

จุฬาลงกรณ์มหาวิทยาลัย
Chulalongkorn University

A Thesis Submitted in Partial Fulfillment of the Requirements
for the Degree of Master of Science in Chemistry
Department of Chemistry
Faculty Of Science
Chulalongkorn University
Academic Year 2023

การรวมตัวเชิงโมเลกุลของอนุภาคนาโนกรดไฮยาลูรอนิกสำหรับการนำส่งยาโดยการจำลองพลวัติเชิงโมเลกุล

นายพิสิฐ เลิศธนะกิจ

จุฬาลงกรณ์มหาวิทยาลัย
CHULALONGKORN UNIVERSITY

วิทยานิพนธ์นี้เป็นส่วนหนึ่งของการศึกษาตามหลักสูตรปริญญาวิทยาศาสตรมหาบัณฑิต
สาขาวิชาเคมี ภาควิชาเคมี
คณะวิทยาศาสตร์ จุฬาลงกรณ์มหาวิทยาลัย
ปีการศึกษา 2566

Thesis Title	MOLECULAR ASSEMBLY OF HYALURONIC ACID NANOPARTICLES FOR DRUG DELIVERY BY MOLECULAR DYNAMICS SIMULATION
By	Mr. Pisit Lerttanakij
Field of Study	Chemistry
Thesis Advisor	Professor PORNTHEP SOMPORNPISUT, Ph.D.

Accepted by the FACULTY OF SCIENCE, Chulalongkorn University in Partial Fulfillment of the Requirement for the Master of Science

..... Dean of the FACULTY OF SCIENCE
(Professor PRANUT POTIYARAJ, Ph.D.)

THESIS COMMITTEE

..... Chairman
(Professor VITHAYA RUANGPORNVISUTI, Ph.D.)
..... Thesis Advisor
(Professor PORNTHEP SOMPORNPISUT, Ph.D.)
..... Examiner
(Associate Professor Pornchai Rojsitthisak, Ph.D.)
..... Examiner
(Associate Professor Somsak Pianwanit, Ph.D.)
..... External Examiner
(Assistant Professor Sunan Kitjaruwankul, Ph.D.)

จุฬาลงกรณ์มหาวิทยาลัย
Chulalongkorn University

อนุภาคนาโน (NPs) ถือว่าเป็นความหวังทางการแพทย์สมัยใหม่ที่สามารถใช้ในการรักษาโรคต่างๆได้ อนุภาคนาโนถูกใช้เป็นตัวพาที่มีประสิทธิภาพสำหรับยาหลากหลายชนิดรวมถึงยาปฏิชีวนะ ยาต้านไวรัส และยาต้านมะเร็ง โดยอนุภาคนาโนจากกรดไฮยาลูรอนิก (HA-NPs) ได้รับความสนใจมากเนื่องจากสมบัติความเข้ากันได้ทางชีวภาพและความสามารถในการย่อยสลายได้ทางชีวภาพที่ยอดเยี่ยม กรดไฮยาลูรอนิก (HA) เป็นพอลิเมอร์ชีวภาพที่มีประโยชน์ในการใช้งานที่หลากหลาย อย่างไรก็ตามการศึกษาเกี่ยวกับการจำลองพลวัติเชิงโมเลกุล (MD) ของอนุภาคนาโนโดยเฉพาะ HA-NPs มีอยู่อย่างจำกัด ในการศึกษานี้ ได้นำ MD มาใช้สำรวจโมเดลการรวมตัวกันของ HA-NPs 2 ประเภทคือ อนุภาคนาโนของกรดไฮยาลูรอนิกที่มีการแทนที่ด้วยหมู่แอซีทิล (AcHA-NPs) และ อนุภาคนาโนของกรดไฮยาลูรอนิก-เซราไมด์ (HACe-NPs) ซึ่งศึกษาในด้านความเสถียรและความสามารถในการดูดซับยา โดยการปรับเปลี่ยนขนาดและจำนวนของโมเลกุลของ HA เพื่อสร้างอนุภาคนาโนภายใต้เงื่อนไขที่แตกต่างกัน ผลการศึกษาพบว่าแบบจำลอง AcHA-NP นำไปสู่โครงสร้างที่จัดเรียงตัวแบบสุ่มหรือโครงสร้างอสัณฐาน ในขณะที่ HACe-NP แสดงโครงสร้างคล้ายไมเซลล์ที่จัดเรียงตัวเป็นระเบียบ โดยทั้งสองประเภทของ HA-NPs แสดงศักยภาพในการเป็นตัวนำพายา เนื่องจากสามารถกักเก็บโมเลกุลดอกซอรูบิซินได้ โดย AcHA-NP ไม่มีบริเวณที่เจาะจงในการจับกับยาเนื่องจากโครงสร้างที่จัดเรียงตัวแบบสุ่ม ในขณะที่ยาอยู่บริเวณรอบแกนที่ไม่ชอบน้ำของ HACe-NP

จุฬาลงกรณ์มหาวิทยาลัย
CHULALONGKORN UNIVERSITY

สาขาวิชา เคมี ลายมือชื่อนิสิต .....

ปีการศึกษา 2566 ลายมือชื่อ อ.ที่ปรึกษาหลัก .....

6370018923 : MAJOR CHEMISTRY

KEYWORD: Hyaluronic acid, Molecular dynamics simulations, self-assembly, Doxorubicin, Drug delivery

Pisit Lerttanakij : MOLECULAR ASSEMBLY OF HYALURONIC ACID NANOPARTICLES FOR DRUG DELIVERY BY MOLECULAR DYNAMICS SIMULATION . Advisor: Prof. PORNTHEP SOMPORNPISUT, Ph.D.

Nanoparticles (NPs) offer a promising approach in modern medicine for the treatment of various diseases. They serve as effective carriers for various drugs including antibiotics, antivirals and anticancer agents. Hyaluronic acid-based nanoparticles (HA-NPs) have been interested owing to their exceptional biocompatibility and biodegradability. Hyaluronic acid (HA) is a natural biopolymer with versatile applications. However, there have been limited numbers of studies on molecular simulations of nanoparticles, particularly HA-NPs. In this study, molecular dynamics simulations were employed to explore molecular models representing the assembly of HA-NPs. Two types of HA-NPs, acetylated hyaluronic acid nanoparticles (AcHA-NPs) and hyaluronic acid-ceramide nanoparticles (HACe-NPs), were assessed for their stability and drug adsorption ability by varying the size and number of HA chains to form the nanoparticle under different conditions. The findings of the study revealed that the AcHA-NP model adopted a random or amorphous structure, whereas the HACe-NP exhibited a well-organized micelles-like structure. Both types of HA-NPs demonstrated potential drug carriers, as doxorubicin molecules were able to bind. It is important to note that AcHA-NP lacked of specific binding site due to its random structure whereas the drug clustered around the hydrophobic core of the HACe-NP.

จุฬาลงกรณ์มหาวิทยาลัย
Chulalongkorn University

Field of Study: Chemistry Student's Signature .....

Academic Year: 2023 Advisor's Signature .....

ACKNOWLEDGEMENTS

Firstly, I would like to thank my advisor, Professor Dr. Pornthep Sompornpisut for his support and advice, which helped me in doing this project and I came to know about so many new things. It has been honored for me to work and learn under his supervision.

I would also like to thank my thesis committee: Professor Dr. Vithaya Ruangpornvisuti, Associate Professor Dr. Somsak Pianwanit, Associate Professor Dr. Pornchai Rojsitthisak, and Assistant Professor Dr. Sunan Kitjaruwankul for offering their time, support, suggestion and review of this document.

I addition, I would like to thank all members of the Center of Excellence in Computational Chemistry (CECC) for their kindness and friendliness over the time of doing the project and research fund from The Development and Promotion of Science and Technology Talents Project (DPST).

Finally, I would like to thank my family and friends for their great support for me.

Pisit Lerttanakij

จุฬาลงกรณ์มหาวิทยาลัย
CHULALONGKORN UNIVERSITY

TABLE OF CONTENTS

Page

ABSTRACT (THAI) iii

ABSTRACT (ENGLISH) iv

ACKNOWLEDGEMENTS v

TABLE OF CONTENTS vi

LIST OF TABLES ix

LIST OF FIGURES x

CHAPTER 1 INTRODUCTION 1

1.1 Cancer disease 1

1.2 Application of nanotechnology to drug delivery 2

1.2.1 Liposomes 4

1.2.2 Solid Lipid Nanoparticles 4

1.2.3 Dendrimers 4

1.2.4 Mesoporous Silica Nanoparticles 5

1.2.5 Nanogels 5

1.2.6 Micelles 6

1.2.7 Polymeric nanoparticles 6

1.3 Hyaluronic acid 8

1.3 Doxorubicin 9

1.4 Literature review 11

1.4 Objectives of research 15

CHAPTER 2 THEORY 16

จุฬาลงกรณ์มหาวิทยาลัย
Chulalongkorn University

2.1 Molecular dynamic simulation 16
2.2 The Newton's Second Law 16
2.3 Molecular mechanical force field 17
2.4 Integration algorithm 18
2.5 The Periodic boundary conditions 20
2.6 Analysis of MD results 21
2.6.1 Radius of gyration 21
2.6.2 Radial pair distribution function 21
CHAPTER 3 METHODOLOGY 22
3.1 Computational software 22
3.1.1 Visual Molecular Dynamics (VMD) 22
3.1.2 Nanoscale Molecular Dynamics (NAMD) 22
3.1.3 CHARMM force field 22
3.1.4 Packmol 23
3.2 Methods 23
3.2.1 Acetylated HA nanoparticle model systems 23
3.2.2 AcHA nanoparticle model in the DMSO-water medium 24
3.2.3 Lipid-conjugated HA nanoparticle model systems 26
3.2.4 HACe nanoparticle model in an aqueous solution 27
3.3 Molecular dynamic simulation 28
3.4 MD trajectory analysis 29
CHAPTER 4 RESULTS AND DISCUSSION 30
4.1 Radius of Gyration Analysis for AcHA-NP Stability 30
4.2 Interaction between AcHA-NPs and solvent 34

จุฬาลงกรณ์มหาวิทยาลัย
Chulalongkorn University

4.3 DOX loading capability of AcHA-NPs 35

4.4 Stability of HACe-NPs 38

4.5 Interaction between HACe-NPs and solvent 40

4.6 Encapsulation of DOX by HACe-NP 41

CHAPTER 5 CONCLUSIONS 44

REFERENCES 47

VITA 53

จุฬาลงกรณ์มหาวิทยาลัย
CHULALONGKORN UNIVERSITY

LIST OF TABLES

Page

Table 1.1 Properties of AC-HA_{LW} nanogels..... 12

Table 3.1 The simulated systems for MD simulation of AcHA-NP..... 25

Table 3.2 The simulated systems for MD simulation of HACe-NP 27

Table 4.1 Average number of contacts between AcHA chains with 3.0 Å cutoff 33

Table 4.2 Calculation of radius of gyration per HA chain..... 34

จุฬาลงกรณ์มหาวิทยาลัย
Chulalongkorn University

LIST OF FIGURES

Page

Figure 1.1 The world map ranking of Cancer as a Cause of Death at Ages <70[1] 2

Figure 1.2 Nanomaterials application in various fields[6] 3

Figure 1.3 Different types of nanocarriers serve as drug delivery[7] 7

Figure 1.4 The structure of hyaluronic acid 8

Figure 1.5 Doxorubicin Pathway in a cancer cell[24] 10

Figure 1.6 (A) The size distribution of AC-HALW nanogels and (B) the nanogels of AC-HALW as observed under a scanning electron microscope[15] 11

Figure 1.7 The radius of gyration (R_g) values for HA molecules with hexyl, dodecyl, and octadecyl substitutions[34] 13

Figure 1.8 RDF graph between HA molecules and (a) H atom and (b) O atom of water for different sizes of HA molecules[35] 14

Figure 1.9 The graph of DOX molecules adsorption by DNA nanotubes at various DOX concentrations[36] 14

Figure 2.1 The force field interaction parameters: bond distance (r), bond angle (θ), torsion angle (φ), and improper torsion angle (ψ) 18

Figure 2.2 Schematic of periodic boundary conditions in 2 dimensions 20

Figure 3.1 Schematic representation of the study workflow 26

Figure 3.2 Schematic representation of the HAce-NP preparation 28

Figure 4.1 The effect of different DMSO-water solvent mixtures on the stability of the AcHA assembly 31

Figure 4.2 MD snapshot showing an assembly of AcHA chains into a globular shape at the initial stage (left) and amorphous structure (middle), and disassembled particles (right) at the end of the simulations 32

จุฬาลงกรณ์มหาวิทยาลัย
Chulalongkorn University

Figure 4.3 The interactions between AcHA and the solvent components. (a) The g(r) plot between the hydroxyl group of AcHA and the hydrogen and oxygen atoms of water. (b) The g(r) between the HA and the carbon and oxygen atoms of DMSO. (c) The g(r) between the oxygen atom of DMSO and the different elements in HA. (d) The g(r) between the oxygen atom of DMSO and the various types of hydrogen atoms in HA. 35

Figure 4.4 The effect of DOX drug on the AcHA-NP size. The R_g profile of the AcHA-NP was calculated from 100 ns simulations in the presence and absence of the DOXdrug. The presence of DOX drug reduced the R_g values of the AcHA-NP, indicating a more compact structure. 36

Figure 4.5 The adsorption of DOX drug on the AcHA-NP surface. The number of adsorbed DOX molecules was counted as a function of time during 100 ns simulations with two different concentrations of DOX: 15 and 30 molecules. As the system approaching an equilibrium, the number of adsorbed DOX molecules on the AcHA surface approaches a similar quantity value for both the DOX30 system and the DOX15 system..... 37

Figure 4.6 MD snapshot showing the adsorption of DOX drug (yellow) on the AcHA-NP surface..... 38

Figure 4.7 The effect of different numbers of HACe molecules on the HACe-NP size. The R_g profile of the HACe-NP was calculated from 100 ns simulations with varying numbers of HACe molecules in the system. The R_g values decreased as the number of HACe molecules increased, indicating a more compact and stable structure of the HACe-NP..... 39

Figure 4.8 The structural stability of the HACe-NP. An assembly of HACe chains into a micelles-like structure at the initial stage (left) and compact structure (middle), and disassembled particles (right) at the end of the simulations..... 39

Figure 4.9 The g(r) plot shows the probability of finding a water molecule at a given distance from the center of mass of the HACe-NP. The g(r) was calculated from 100 ns simulations with different numbers of HACe molecules in the system. The

จุฬาลงกรณ์มหาวิทยาลัย
Chulalongkorn University

absence of a peak in the g(r) plot within the first 10Å suggests that there is no water present in the inner or hydrophobic core of the HACe nanoparticle. 40

Figure 4.10 The effect of DOX drug on the HACe-NP size and stability..... 42

Figure 4.11 The encapsulation of the DOX drug on the HACe-NP surface. The distance between the center of mass of the HACe-NP and the center of mass of each DOX molecule (DOX1, DOX2, DOX3 and DOX4) in the system was calculated from 50 ns simulations. The distance between the center of mass of the HACe-NP and the oxygen atom O1 of HACe was also calculated to estimate the size of the inner core of the nanoparticle model. The distance values indicate how close the DOX drug to the inner hydrophobic core of the HACe-NP..... 42

Figure 4.12 MD snapshot showing the encapsulation of DOX drug (yellow) on the AcHA-NP surface..... 43

จุฬาลงกรณ์มหาวิทยาลัย
Chulalongkorn University

CHAPTER 1

INTRODUCTION

1.1 Cancer disease

Cancer is undeniably one of the major causes of death worldwide and it is a significant public health problem. In 2020, there were an estimated 19.3 million new cancer cases and almost 10.0 million cancer deaths, according to the World Health Organization (WHO). Cancer's impact is far-reaching and deeply concerning. In 112 out of 183 countries, cancer ranks as a leading cause of death before the age of 70, frequently occupying the first or second rank in terms of mortality (**Figure 1.1**) [1]. Cancer is a term used to describe a group of diseases characterized by the uncontrolled proliferation and spread of abnormal cells within the body. These cells can invade and destroy surrounding healthy tissues, and they may also migrate to other parts of the body through the bloodstream or lymphatic system, forming new tumors in a process known as metastasis. This disease can strike in various forms, affecting multiple organs and tissues. Cancer is not a singular entity but a spectrum of conditions, each with its own characteristics, challenges, and treatment options. It can be a life-threatening menace if not detected and addressed in its early stages. Cancer's causes are complex, but several key factors drive its development. Age is a significant contributor, with cancer becoming more prevalent as people grow older, emphasizing the importance of regular screenings. Genetic mutations, often linked to exposure to carcinogenic substances, hereditary factors, and radiation, can increase susceptibility to cancer, highlighting the need for genetic counseling and family medical history awareness. Lifestyle choices, like smoking and excessive alcohol consumption, also elevate specific cancer risks.

จุฬาลงกรณ์มหาวิทยาลัย
CHULALONGKORN UNIVERSITY

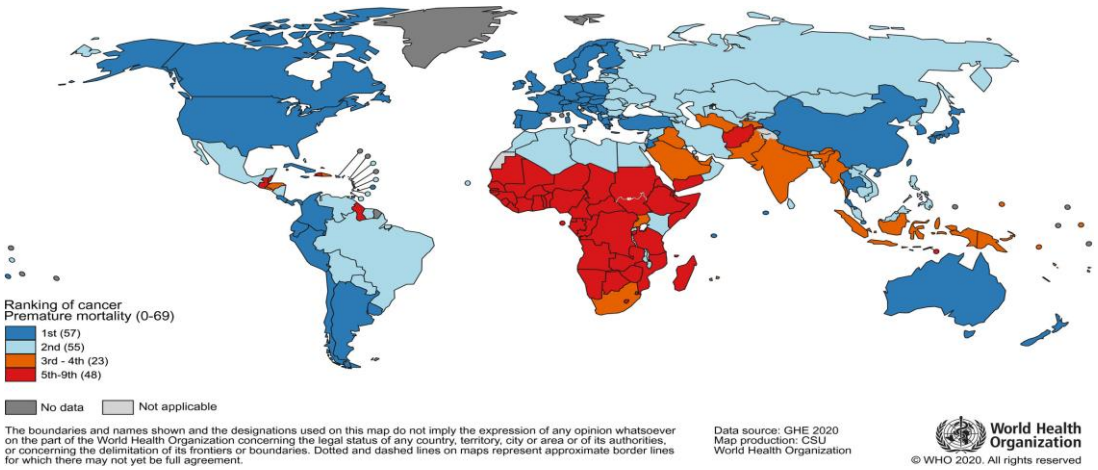

Figure 1.1 The world map ranking of Cancer as a Cause of Death at Ages <70[1]

In the treatment of cancer, various methods are available such as chemotherapy and non-pharmaceutical treatments such as radiation therapy, surgery, hyperthermia, and stem cell therapy. Some cases may also involve a combination of these methods[2]. However, each method has its disadvantages. For example, chemical treatment methods are hampered by the water solubility of drugs due to their high lipophilicity and lack of specificity for cancer cells, which can lead to drug side effects[3, 4]. In an attempt to minimize the disadvantages of chemotherapy, targeted therapy has been employed to enhance specificity for cancer cells and reduce the side effects on normal cells. Targeted therapy can be developed through various methods, in which one of these involves the use of nanotechnology as drug carriers to improve the solubility of cancer drugs and enhance specificity for cancer cells[5].

จุฬาลงกรณ์มหาวิทยาลัย
Chulalongkorn University

1.2 Application of nanotechnology to drug delivery

Nanotechnology involves using materials on atomic, molecular, and supramolecular scales. These materials are called nanomaterials. Nanomaterials have unique properties due to their small dimensions (1–100 nm). They possess high electrical properties, mechanical and thermal stability, surface area, as well as optical and magnetic properties[6]. In medicine, nanomaterials can be employed for various

purposes such as nanomachinery, antibacterial agent, nanoimaging, tissue engineering and drug delivery (**Figure 1.2**).

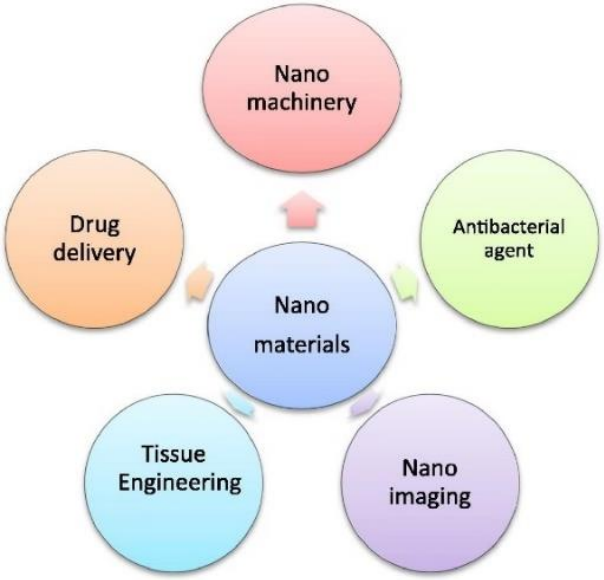

Figure 1.2 Nanomaterials application in various fields[6]

For drug delivery, the incorporation of nanotechnology into drug delivery systems offers several advantages. One of the most significant benefits is the ability to enhance drug bioavailability. Many types of drugs, especially those with poor water solubility, can pose challenges in drug delivery to the target within the body. Nanomaterials such as nanoparticles can encapsulate drugs and improve their solubility and stability, thereby increasing the percentage of the drug that can reach its target. Moreover, by engineering nanoparticles to target specific cells, tissues, or organs, drug delivery is made highly precise. This approach not only enhances treatment efficacy but also lowers the risk of damage to healthy tissues, resulting in reduced off-target effects and the need for lower drug dosages. In addition, nanoparticles can be designed to release their cargo gradually and consistently over an extended period. This controlled release mechanism maintains therapeutic drug concentrations in the body, eliminating the need for frequent dosing. Furthermore, nanotechnology enables the co-delivery of multiple drugs within a single carrier. It creates possibilities for synergistic effects, which can be particularly beneficial in

จุฬาลงกรณ์มหาวิทยาลัย
Chulalongkorn University

treating complex diseases. Nanomaterials for drug delivery can be in various forms based on their advantage and properties[7].

1.2.1 Liposomes

Liposomes are the earliest nanoparticles used for delivery purposes. Their main composition consists of phospholipids. Liposomes can comprise a single or multiple layers of phospholipids surrounding an aqueous core. The composition of a liposome can be customized to meet specific requirements, such as lipid composition, charge, size, and antigen location. The advantage of liposomes is their ability to encapsulate drugs. Hydrophobic drugs can be incorporated into the lipid bilayer, while hydrophilic drugs can be enclosed within the aqueous core of the liposome. This dual compatibility allows liposomes to carry many therapeutic agents, including chemotherapy drugs, antibiotics, and genetic materials like DNA and RNA. However, liposomes also have limitations, such as potential instability over time, difficulty in scale-up production, and challenges in achieving precise control over drug release kinetics[8].

1.2.2 Solid Lipid Nanoparticles

Solid Lipid Nanoparticles (SLNs) consist of biocompatible and biodegradable solid lipids, which are lipids that remain solid at body temperature. The lipids are stabilized by surfactants that coat the particle surface, preventing aggregation and ensuring stability. The selectivity of SLNs can be improved by modifying their surface with molecules that specifically bind to targets, allowing SLNs to encapsulate various drugs, including both hydrophobic and hydrophilic compounds. The drugs can be embedded within the lipid matrix or adsorbed onto the particle surface, depending on their solubility properties. However, SLNs also have some limitations, such as potential drug leakage during storage, batch-to-batch variability, and challenges related to scale-up production[9].

1.2.3 Dendrimers

Dendrimers are highly structured, nanoscale macromolecules with well-defined and symmetric branching patterns. Dendrimers have a central

จุฬาลงกรณ์มหาวิทยาลัย
Chulalongkorn University

core from which multiple branches or generations radiate outward in a symmetric and tree-like shape. Dendrimers can be functionalized on their terminal with ligands, antibodies, or other molecules that enable them to target specific cells or tissues. The advantage of dendrimers is the precise control over drug release kinetics. The rate of drug release can be tailored by modifying dendrimer properties, such as size, surface charge, and functional groups. This control is crucial for achieving sustained or targeted drug delivery. However, they also have limitations. They are complex and expensive to synthesize, may exhibit toxicity and immunogenicity concerns, and have size constraints that affect their tissue penetration. Furthermore, biodegradability and clinical translation challenges exist, and they may have limited drug loading capacity[10].

1.2.4 Mesoporous Silica Nanoparticles

Mesoporous Silica Nanoparticles (MSNs) are a class of nanomaterials with a unique porous structure composed primarily of silicon dioxide. These nanoparticles possess a network of nanoscale pores with uniform sizes, typically ranging from 2 to 50 nanometers, and high surface area-to-volume ratios. The porous structure of MSNs enables the loading of various types of drugs, including hydrophobic and hydrophilic compounds. Drugs can be physically adsorbed onto the internal surface of the pores or chemically bonded to the silica framework, providing flexibility in drug loading. The advantage of MSNs is the control over drug release kinetics. The release rate can be adjusted by altering the size and characteristics of the pores, as well as by modifying the surface properties of the nanoparticles. However, MSNs also have limitations such as potential aggregation, limited loading capacity for certain drugs, and potential cytotoxicity concerns related to surface functionalization or trace impurities[11].

1.2.5 Nanogels

Nanogels are crosslinked hydrogel particles on the nanometer scale. Hydrogels are three-dimensional, water-swollen polymer networks that absorb and retain large amounts of water or biological fluids. Nanogels are

composed of hydrophilic polymers that form a porous, crosslinked structure. The advantage of nanogels is their well-absorbing capacity for water or biological fluids, allowing them to encapsulate and retain drugs, proteins, or nucleic acids within their porous matrix. Nanogels provide the ability to control drug release. Drug release rates can be controlled by adjusting the polymer composition, crosslinking density, and environmental conditions, such as pH or temperature. Nanogels can be functionalized with targeting ligands or antibodies to achieve site-specific drug delivery. They can encapsulate various drugs, including hydrophobic and hydrophilic small molecules and macromolecules like proteins and nucleic acids. However, nanogels also have limitations such as their stability, potential drug leakage during storage, and challenges in scale-up production[12].

1.2.6 Micelles

Micelles are self-assembling structures formed by amphiphilic molecules in a solution. These amphiphilic molecules have both hydrophilic and hydrophobic regions. In a solution, these molecules spontaneously organize themselves into micelles. Micelles are typically spherical nanoparticles with a hydrophilic shell and a hydrophobic core. Micelles can solubilize hydrophobic drugs within their hydrophobic cores. This property is particularly useful for improving the solubility of poorly water-soluble drugs, as it allows them to be transported effectively in the bloodstream. They can provide controlled drug release by changing the composition of the micelles, such as the length of the hydrophobic tails, the type of amphiphilic molecules used, or the environmental conditions. Micelles can be modified by ligands or antibodies on their surface for specific targeting. The limitations of micelles in drug delivery are potential instability and difficulty in achieving high drug loading[13].

1.2.7 Polymeric nanoparticles

Polymeric nanoparticles are typically made from synthetic or natural polymers. Polymeric nanoparticles can encapsulate various types of drugs, including small molecules or macromolecules, and even imaging agents.

Hydrophobic drugs can be incorporated into many parts of nanoparticles such as polymer matrix, aqueous core or onto the particle surface. The significant advantages of polymeric nanoparticles are their ability to provide controlled and sustained drug release. The release kinetics can be precisely tailored by adjusting factors such as polymer composition, molecular weight, and the method of nanoparticle preparation. They can be functionalized with targeting ligands, antibodies, or peptides that enable them to bind specifically to a target. Polymeric nanoparticles are also relatively easy to formulate and can be scaled up for mass production. The limitations of polymeric nanoparticles are potential instability and difficulty in achieving high drug loading[14].

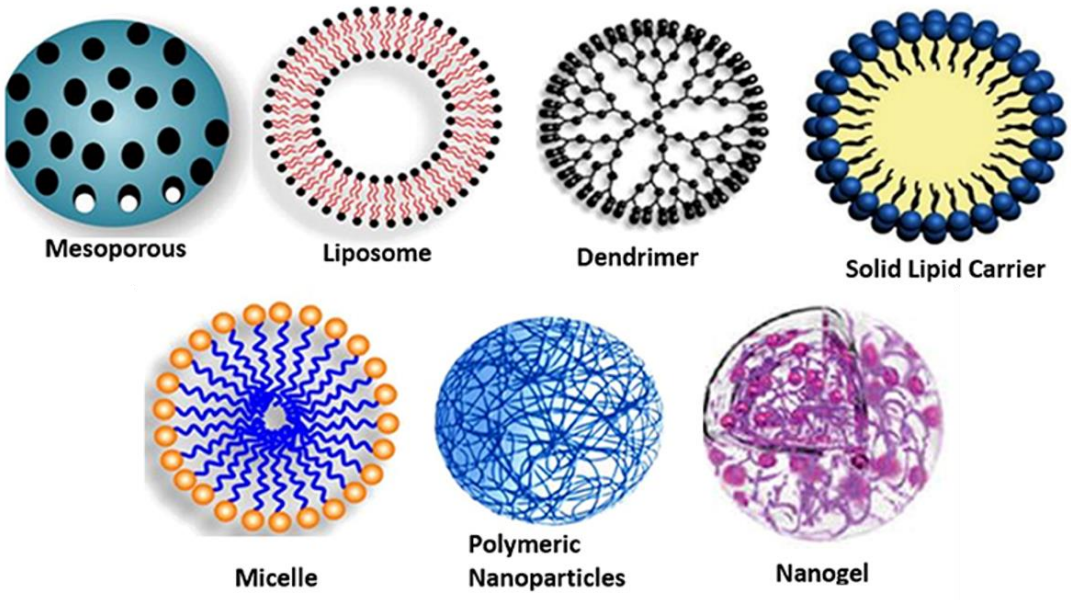

Figure 1.3 Different types of nanocarriers serve as drug delivery[7]

Polymeric nanoparticles and micelles have unique properties that make them attractive for development in medical applications. These nanocarriers can be easily prepared through self-assembly in a solution, enabling scalable production. The limitations of polymeric nanoparticles and micelles include potential instability and challenges in achieving high drug quantities, which can be addressed or reduced by

modifying ingredient molecules or polymers that are used as starting materials. Due to these advantages, there has been a focus on researching polymeric nanoparticles using hyaluronic acid as nanocarriers for delivering doxorubicin[15], which serves as an anticancer drug. Additionally, hyaluronic acid has been used as a starting material in the production of micelles for drug delivery purposes[16].

1.3 Hyaluronic acid

Hyaluronic acid (HA) is a glycosaminoglycan, a type of carbohydrate polymer with negatively charged groups. The smallest subunit of HA is a disaccharide composed of two sugar molecules: β-D-glucuronic acid (GlcA) and β-D-N-acetylglucosamine (GlcNAc), linked together by a glycosidic bond. Within the HA molecule, there are two types of glycosidic bonds: β(1,3) and β(1,4), arranged alternately, as shown in **Figure 1.4** This specific arrangement contributes to the robust and linear nature of HA molecules, resulting in long, unbranched polymers[17].

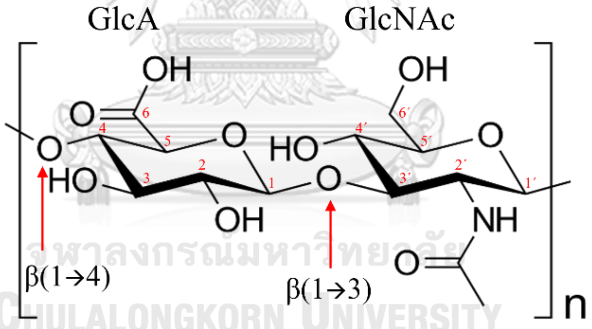

Figure 1.4 The structure of hyaluronic acid

HA serves a crucial role in numerous biological processes, encompassing cell signaling, wound healing, tissue regeneration, morphogenesis, matrix organization, and pathobiology. It is a vital constituent of skin, cartilage, connective, epithelial, and neural tissues. Hyaluronic acid possesses remarkable physico-chemical characteristics, such as biocompatibility, biodegradability, and outstanding water retention capacity, . These have established it as an ideal substance employed in various medical, pharmaceutical, nutritional, and cosmetic applications[18, 19]. HA has been found to specifically bind with receptors that are overexpressed on cancer cells, such as

CD44[20] and RHAMM3[21]. Therefore, HA can be utilized as a targeted drug delivery system, specifically interacting with cancer cells. HA can be used in nanoscale materials like nanoparticles and nanogels, which are easy to prepare by self-assembly of HA molecules. However, due to the large size and excellent water solubility property of HA, it often requires modification by adding low polarity groups to reduce water solubility and using low molecular-weight HA is essential to create nanoparticles suitable for delivering anticancer drugs[22].

1.3 Doxorubicin

Doxorubicin is a cytotoxic anthracycline antibiotic that was first discovered through extraction from *Streptomyces peucetius var. Caesius*[23]. In addition to inhibiting bacteria, DOX is an effective anticancer drug that is widely used in chemotherapy. The mechanism of action for the anticancer effects of DOX occurs within the cell nucleus. DOX works by inhibiting topoisomerase II, an important enzyme for relaxing DNA supercoils during DNA transcription and replication. Moreover, DOX can intercalate between base pairs of DNA. Both mechanisms lead to DNA damage and result in cell apoptosis. In addition, DOX can undergo a one-electron reduction by several oxidoreductases to form a DOX-semiquinone radical and cause damage to cellular membranes, DNA and proteins. However, DOX still has the primary side effect of cardiotoxicity, with its potential to cause heart problems. This may manifest as harm to the cardiac muscle or the development of heart failure. However, the exact mechanism of this side effect is not yet fully understood[24]. Therefore, the use of targeted drug delivery systems becomes essential in the treatment of cancer with DOX in chemotherapy to minimize side effects.

จุฬาลงกรณ์มหาวิทยาลัย
CHULALONGKORN UNIVERSITY

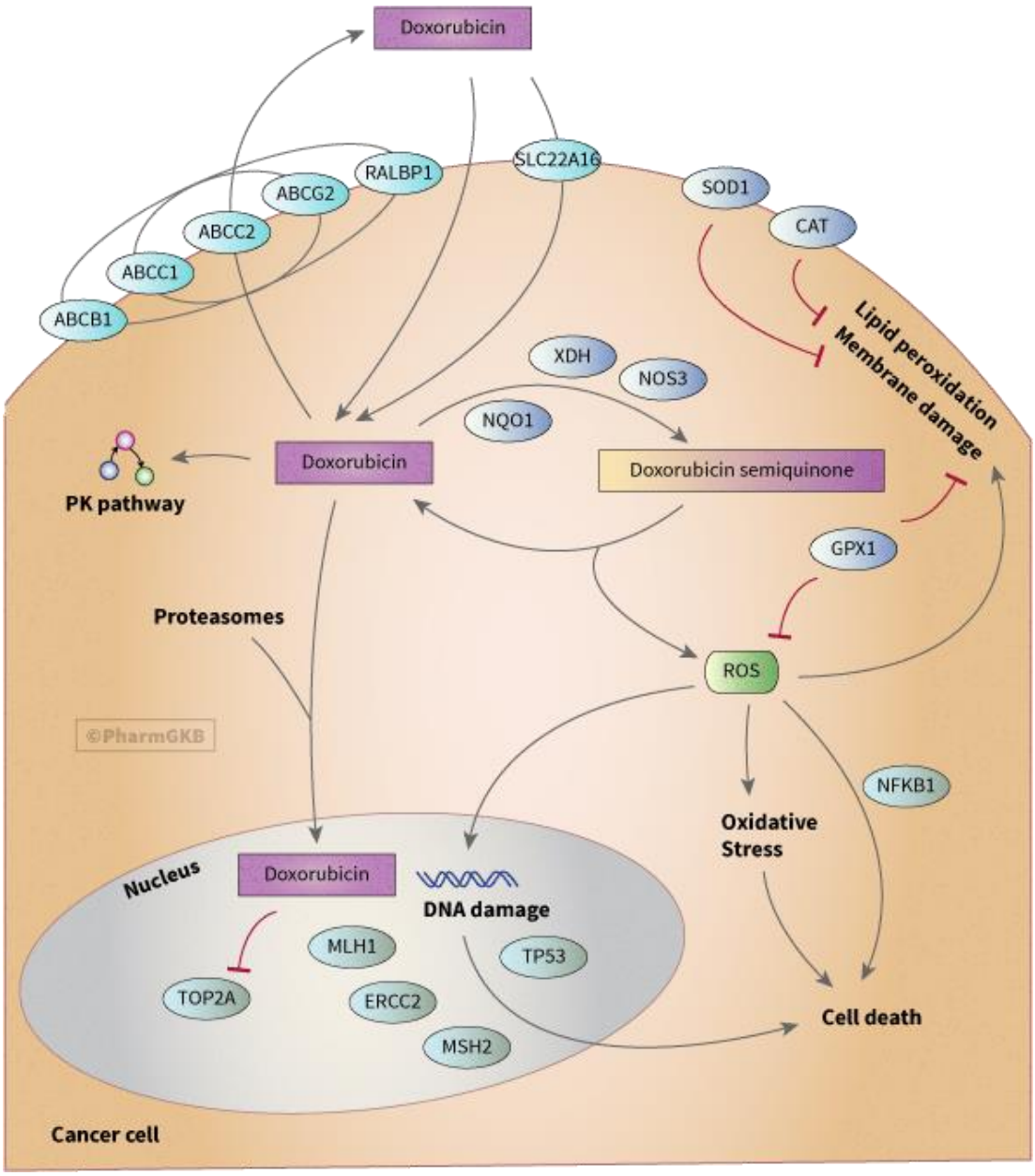

Figure 1.5 Doxorubicin Pathway in a cancer cell[24]

In research studies, it has been reported that acetyl groups were successfully incorporated into HA molecules with a molecular weight of less than 50 kDa. These modified HA molecules, known as acetylated hyaluronic acid (AC-HA), have the ability to self-assemble into nanoparticles. These AC-HA nanoparticles can be used as drug delivery carriers for the anticancer drug DOX, allowing it to be delivered

effectively into cancer cells[15]. Moreover, there are reports of HA being modified with hydrophobic polymers to create amphiphilic polymers. These amphiphilic polymers can self-assemble into micelles[16]. However, there is no research on the structural characteristics of these AC-HA nanoparticles and HA micelles, as well as no study on the atomic-level interaction ratios between those nanocarriers and DOX. Therefore, this research is focused on studying the structure of AC-HA nanoparticles and HA micelles, and the interaction with DOX at the atomic level. The chosen methodology for this investigation is molecular dynamics (MD) simulations.

1.4 Literature review

In 2010, W. Park and co-worker[15] developed a method for synthesizing nanogels using low molecular weight hyaluronic acid (LMWHA) molecules, which refers to HA with a molecular weight of less than 50 kDa. They achieved this by modifying acetyl groups onto the LMWHA molecules through an acetylation reaction, resulting in acetylated low molecular weight hyaluronic acid (AC-HALW). It was observed that AC-HALW could self-assemble into nanogels when dissolved in a solvent like dimethyl sulfoxide (DMSO). The properties of the nanogels formed by the self-assembly of AC-HALW are shown in **Figure 1.6**.

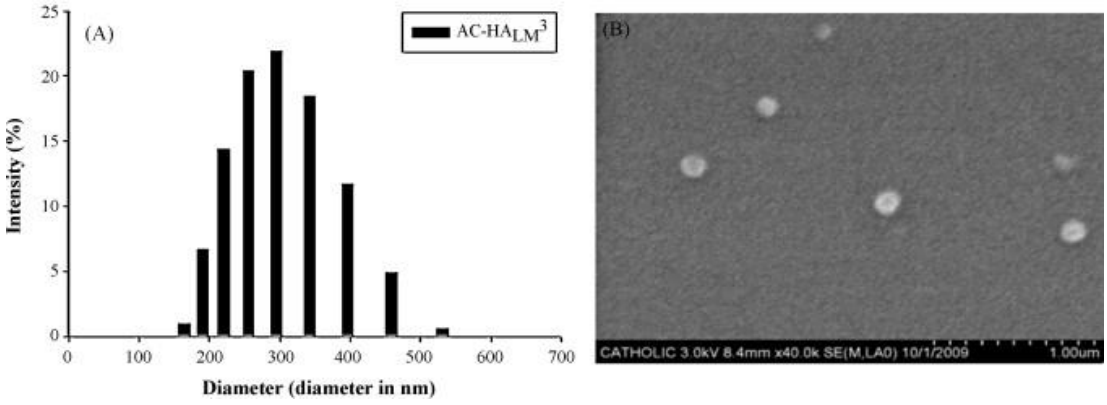

Figure 1.6 (A) The size distribution of AC-HALW nanogels and (B) the nanogels of AC-HALW as observed under a scanning electron microscope[15]

Furthermore, the researchers investigated the impact of the degree of acetylation on the properties of the resulting hydrogels. They studied different levels of acetyl group substitution at 0.84, 2.09, and 2.63 moles per subunit of HA. Additionally, they examined the loading and release of the anticancer drug DOX within the AC-HALW nanogels. The study results are summarized in **Table 1.1**.

Table 1.1 Properties of AC-HA_{LW} nanogels

Sample	Degree of substitution	Particle size (nm.)	CAC* (mg/mL)	DOX-loaded particle size (nm)	Drug-loading efficiency (wt%)
AC-HA_{LM}1	0.84	447 ± 8.	0.07	226 ± 8	59.25 ± 0.17
AC-HA_{LM}2	2.09	290 ± 4	0.06	208 ± 3	83.46 ± 5.23
AC-HA_{LM}3	2.63	275 ± 4	0.05	215 ± 1	93.10 ± 3.21

***Critical aggregation concentration**

The study of the atomic structure of HA was first successful in 1980. Atkins, Meader, and Scott[25] published research on the solid-state structure of HA using X-ray crystallography. The result shows that HA has a helical structure. Subsequently, several studies have investigated the structure of HA in a solution state, using computational and theoretical studies. These investigations include molecular dynamics simulations, Monte-Carlo simulations, quantum chemical calculations, and nuclear magnetic resonance spectroscopy[26-33]. However, most of these research works have primarily focused on the structure of individual HA molecules.

จุฬาลงกรณ์มหาวิทยาลัย
Chulalongkorn University

In 2018, W. M. Payne and co-worker[34] published a study on the self-assembly of HA molecules modified with hexyl, dodecyl, and octadecyl groups in an aqueous solution using molecular dynamics simulations. They analyzed the formation of nanoparticles by radius of gyration. They found that the self-assembly of HA molecules with different modifiers depends on the degree of hydrophobicity of the molecules and the internal stress within the molecules. HA molecules modified with

dodecyl groups had a higher radius of gyration compared to those modified with hexyl and octadecyl groups. Because the dodecyl group is less hydrophobic than the octadecyl group, and it has higher internal stress within the HA molecules compared to the hexyl group. This makes the HA with dodecyl groups less ability to self-association compared to the HA with hexyl and octadecyl groups when comparing their radius of gyration as shown in **Figure 1.7**.

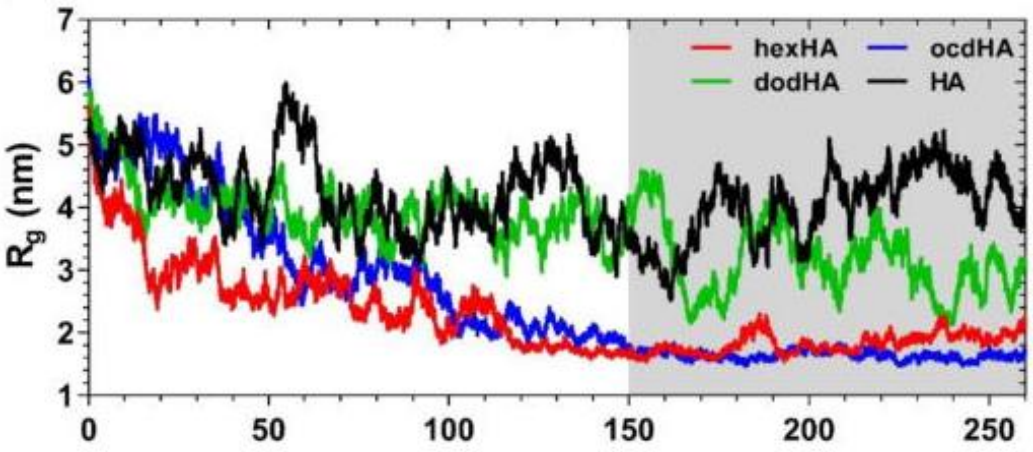

Figure 1.7 The radius of gyration (R_g) values for HA molecules with hexyl, dodecyl, and octadecyl substitutions[34]

In 2020, P. Taweechat and his co-workers[35] conducted a study comparing the hydration properties of HA molecules in different sizes using molecular dynamics simulations. They analyzed the water density at different distances from the HA molecules using radial pair distribution function (RDF) analysis. The results of the RDF analysis between HA molecules and the oxygen (O) and (H) atoms of water showed that the water density around HA molecule decreases with increasing sizes of HA molecules. Furthermore, from the position of the first hydration shell, they found that the size of the HA molecule does not affect the position of the first hydration shell. When comparing the distance of the first hydration shell for both RDF graphs, it was observed that the RDF graph of the HA molecule and the O atom of water had the same position as the RDF graph of the HA molecule and the H atom. It indicates that HA molecules can act as both hydrogen bond donors and acceptors, as shown in **Figure 1.8**.

จุฬาลงกรณ์มหาวิทยาลัย
Chulalongkorn University

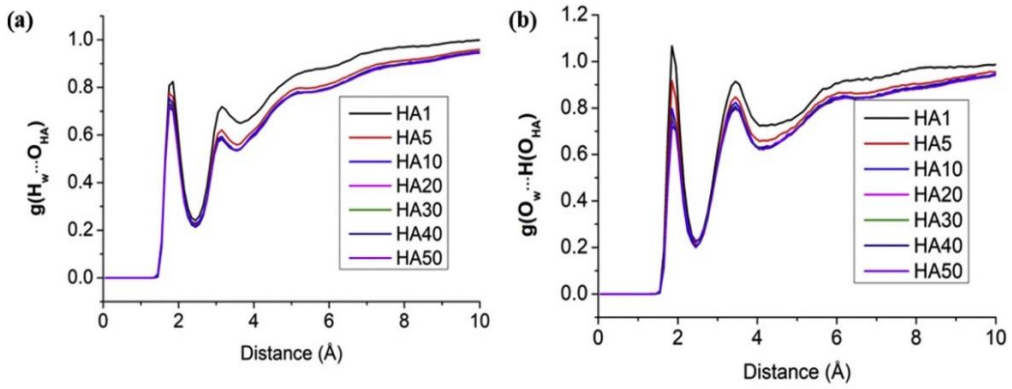

Figure 1.8 RDF graph between HA molecules and (a) H atom and (b) O atom of water for different sizes of HA molecules[35]

In 2017, Liang, Shen and Wang[36] conducted a study on the adsorption of DOX molecules onto DNA nanotubes at different DOX concentrations using molecular dynamics simulations. The analysis involved comparing the number of drugs adsorbed onto DNA nanotubes with the criterion that the distance between the center of mass of DOX and the DNA nanotube should not exceed 0.7 nanometers. The results indicated that when the DOX concentration increased, the number of adsorbed drugs also increased. Moreover, the maximum number of DOX molecules adsorbed onto DNA nanotubes was determined when the adsorption did not increase further with increasing DOX concentration, as shown in **Figure 1.9**.

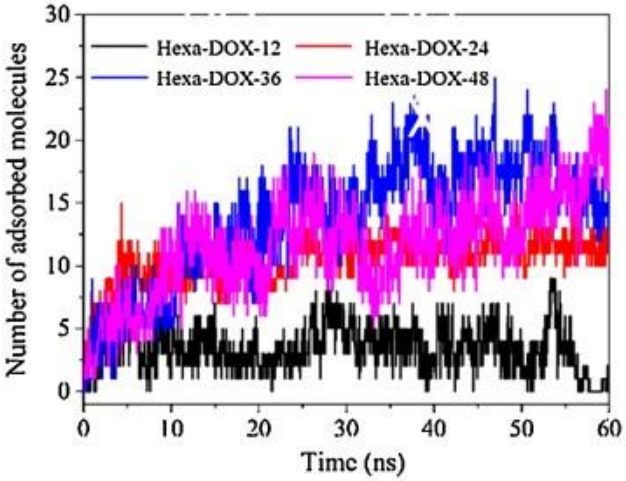

Figure 1.9 The graph of DOX molecules adsorption by DNA nanotubes at various DOX concentrations[36]

1.4 Objectives of research

1.4.1 To Investigate the structure and stability of hyaluronic acid nanoparticles and analyze the intramolecular interactions within the hyaluronic acid nanoparticles in solution using molecular dynamics simulation techniques.

1.4.2 To study the interactions between hyaluronic acid nanoparticles and the anticancer drug doxorubicin.

จุฬาลงกรณ์มหาวิทยาลัย
Chulalongkorn University

CHAPTER 2

THEORY

2.1 Molecular dynamic simulation

MD simulations have been shown to be a powerful tool for investigating biological molecules at the atomic level. MD provides insight into HA nanocarrier structural stability and evolution over time. Moreover, MD simulation can be used to investigate the interaction of HA nanocarrier with drugs to explore of their potential as drug carriers and to study their effectiveness in drug delivery systems.

2.2 The Newton's Second Law

MD simulation is a technique that relies on the numerical integration of Newton's second law of motion to predict the dynamic behavior of particles in a physical system[37]. This technique generates the motion of particles as a function of time by taking into account physical interactions between particles present in the system. The foundation of MD simulation lies on the Newton's second law (**equation 2.1**), which relates the force acting on a particle to its mass and acceleration. The force acting on particle i^{th}, F_i can be described as a product of an acceleration a_i and its mass m_i. Acceleration in the **equation 2.2** can be defined as the second derivative of position r_i with respect to a change in time or the first derivative of velocities v_i over time (**equation 2.3**). The forces that influence the motion of particles within an MD simulation are derived from the potential energy (U) of the system. The force acting on each particle is computed as the gradient of the potential energy with respect to changes in particle positions (**equation 2.4**). Particle positions and velocities of each particle in the next time step are determined by specific inter-atomic potential energy and temperature-defined kinetic energy, respectively. During MD simulation, successive configurations are called dynamic trajectory which is composed of time-dependent positions and velocities of the particles in the system.

จุฬาลงกรณ์มหาวิทยาลัย
CHULALONGKORN UNIVERSITY

$$F_i = m_i a_i \tag{2.1}$$

$$\frac{d^2 r_i}{dt^2} = \frac{F_i}{m_i} \tag{2.2}$$

$$\frac{dv_i}{dt} = \frac{F_i}{m_i} \tag{2.3}$$

$$F_i = -\frac{\partial U}{\partial r_i} \tag{2.4}$$

2.3 Molecular mechanical force field

In molecular mechanic theory, the potential energy of the system is a function of atomic position. Atomistic models are considered as spheres connected by bonds as springs. Atoms that are greater than two bonds apart can interact through van der Waals attraction, steric repulsion, and electrostatic attraction/repulsion. The potential energy can be described by the sum of individual two-body interacting terms[38, 39]. A general form of the molecular mechanic potential function is shown in **equation 2.5.**

$$U = \sum_{bond} k_b (r - r_0)^2 + \sum_{angle} k_\theta (\theta - \theta_0)^2 + \sum_{torsion} k_\phi [1 + \cos(n\phi + \delta)] + \sum_{improper} k_\psi (\psi - \psi_0)^2 + \sum_{vdW} \epsilon \left(\frac{A_{ij}}{r_{ij}^6} - \frac{B_{ij}}{r_{ij}^{12}} \right) + \sum_{elec} \frac{q_i q_j}{4\pi\varepsilon_0 r_{ij}} \tag{2.5}$$

จุฬาลงกรณ์มหาวิทยาลัย
Chulalongkorn University

Where k_b, k_θ, k_φ and k_ω refer to the force constant of the potential functions associated with bond stretching, angle, torsion angle, and improper torsion, respectively. The ϵ, A_{ij} and B_{ij} are the coefficients for Van der Waals term. The distance r_{ij} defines a separation between the particle i^{th} and j^{th} with partial atomic charge q_i and q_j, ε_0 is the dielectric constant. The first four terms are used to calculate the bonded energy. The fifth term is known as the Lennard-Jones potential

function. The last term is electrostatic energy. All parameters defined in **equation 2.5** equation are called force-field parameters.

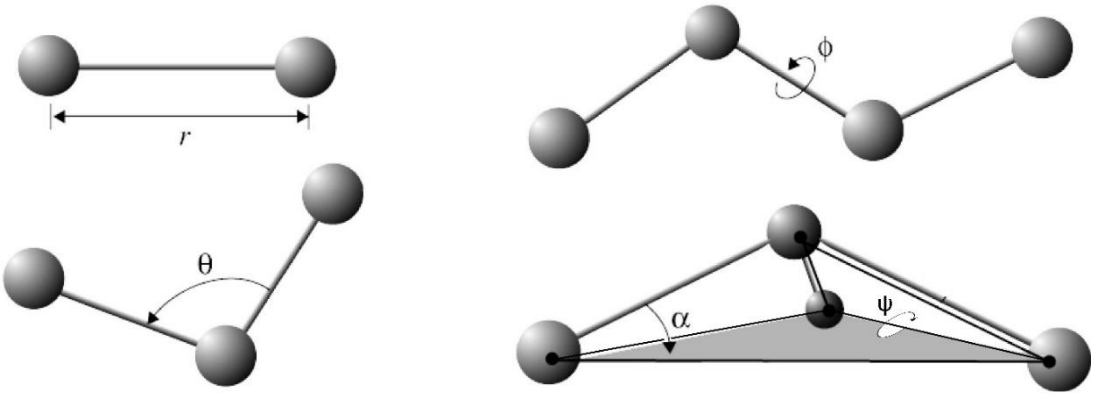

Figure 2.1 The force field interaction parameters: bond distance (r), bond angle (**θ**), torsion angle (**φ**), and improper torsion angle (**ψ**)

2.4 Integration algorithm

MD simulations are employed to study the dynamic behavior of molecules over time. However, the complexity of molecular systems often makes it impossible to solve analytical solutions for the equations of motion governing these systems. This is where numerical methods are essential. In Molecular Dynamics, the trajectory is divided into small steps **δ**t. The Vervet algorithm[40] has to be used to solve for the next time step of particle position and velocity. First, extend the position at t + **δ**t and t - **δ**t in the Taylor series as **equation 2.6** and **2.7**

$$r(t+\delta t) = r(t) + v(t)\delta t + \frac{1}{2}a(t)\delta t^2 + \frac{1}{6}b(t)\delta t^3 + O(\delta t^4) \quad (2.6)$$

$$r(t-\delta t) = r(t) - v(t)\delta t + \frac{1}{2}a(t)\delta t^2 - \frac{1}{6}b(t)\delta t^3 + O(\delta t^4) \quad (2.7)$$

Where r is position, v is velocity, a is acceleration, b is 3rd derivative of position, O is global error, and t is time. Adding **equation 2.6** with **equation 2.7** will give the new **equation 2.8.**

$$r(t + \delta t) = 2r(t) - r(t - \delta t) + a(t)\delta t^2 \qquad (2.8)$$

The **equation 2.8** is used to calculate the new position at time t + **δ**t

The subtraction of **equation 2.6** from **equation 2.7** yields the formula for calculating the velocity at time t as shown in **equation 2.9.**

$$v(t) = \frac{r(t + \delta t) - r(t - \delta t)}{2\delta t} \qquad (2.9)$$

However, **equation 2.9** required not only the position at time t + **δ**t but also at t – **δ**t to calculate velocity, which poses a problem. This is because the Verlet algorithm assumes constant acceleration over the time interval, but there may be forces acting on the particle during that time. To address this issue, the Velocity Verlet algorithm as **equation 2.10** and **equation 2.11** is employed to tackle such problems.

$$r(t + \delta t) = r(t) + v(t)\delta t + \frac{1}{2}a(t)\delta t^2 \qquad (2.10)$$

$$v(t + \delta t) = v(t) + \frac{a(t) + a(t + \delta t)}{2}\delta t \qquad (2.11)$$

จุฬาลงกรณ์มหาวิทยาลัย
CHULALONGKORN UNIVERSITY

The standard scheme of this algorithm can be as follows. First, calculate **equation 2.12**.

$$v\left(t + \frac{\delta t}{2} \right) = v(t) + \frac{a(t)\delta t}{2} \qquad (2.12)$$

Then calculate the acceleration form forces on the particle at time t + **δ**t and calculate **equation 2.13.**

$$v(t + \delta t) = v\left(t + \frac{\delta t}{2} \right) + \frac{a(t + \delta t)\delta t}{2} \qquad (2.13)$$

2.5 The Periodic boundary conditions

Periodic boundary conditions (PBC) are a computational method that introduces repeating unit cells into a simulation system. With PBC, even a system containing only a few hundred atoms behaves as if it were infinitely large. This approach reduces the surface effects of any finite sample of matter and ensures that the internal structure of the sample is influenced more by bulk forces than surface forces. The simulation system is modeled as a suitable box. All atoms within the box are duplicated in all directions, creating an infinite lattice of image cells as shown in **Figure 2.2**. These image cells maintain the same size and shape as the primary cells. In open boundaries, particles are free to enter or exit any cell. When a particle moves out of a cell, its corresponding image particle enters the cell from the opposite side[41].

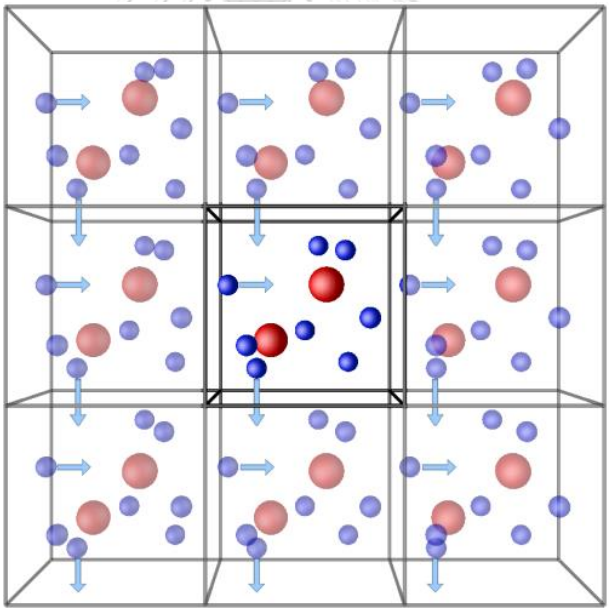

Figure 2.2 Schematic of periodic boundary conditions in 2 dimensions

The thermodynamic properties of a system under PBC are computed using statistical mechanics. The ensemble is an idealization composed of many or infinite virtual copies of a system and each of them represents a possible state reflecting the

real system. The PBC is a molecular ensemble. The isobaric-isothermic ensemble is widely used to mimic the conditions of many real-world experiments. In this ensemble, the system's volume is allowed to fluctuate while maintaining a constant pressure, and energy. In simpler terms, the ensemble is defined by three constants: number of atoms (N), pressure (P), and temperature (T). Therefore, this ensemble is referred to as the NPT ensemble[42].

2.6 Analysis of MD results

The trajectory generated by MD contains information typically used for a subsequent analysis to obtain meaningful structural and thermodynamical properties of the system such as root mean square deviation, radius of gyration, and Radial pair distribution function[43, 44].

2.6.1 Radius of gyration

The Radius of gyration (R_g) describes the distribution of mass with respect to its center of mass. R_g is the root mean squared distance from the center of mass. It can be calculated by using equation 2.15.

$$R_g = \left[\frac{1}{\sum_{i=1}^{N} m_i} \sum_{i=1}^{N} m_i \| r_i - \bar{r} \|^2 \right]^{\frac{1}{2}} \quad (2.15)$$

Where r_i is the position of i^{th} atom, m_i is the mass of i^{th} atom and $\bar{r}$ is the position of center of mass.

จุฬาลงกรณ์มหาวิทยาลัย
Chulalongkorn University

2.6.2 Radial pair distribution function

The Radial pair distribution function (RDF) is one of the tools in statistical mechanics that demonstrates a probability to find a particle at distance r away from a given reference particle. This function is determined by calculating the average number of particles within each shell at the distance r from any given point. Then normalized by dividing it by the total number of particles, the volume of each shell, and the average density of particles within the system.

CHAPTER 3

METHODOLOGY

3.1 Computational software

3.1.1 Visual Molecular Dynamics (VMD)

VMD is a useful program for molecular modeling and simulation study of biological molecules. VMD supports computers that run on Windows, MacOS X, and Unix operating system. It has been developed by Theoretical and Computational Biophysics Group at the Beckman Institute for Advanced Science and Technology, University of Illinois at Urbana–Champaign[45, 46]. This program is distributed free of charge, including the source code. (https://www.ks.uiuc.edu/Research/vmd/)

3.1.2 Nanoscale Molecular Dynamics (NAMD)

NAMD is a software that performs advanced simulations and calculations to study the behavior and energy interactions of large biological molecular systems using parallel processing, enabling efficient and high-performance molecular dynamics research. It is free software developed by the Theoretical and Computational Biophysics Group at the Beckman Institute for Advanced Science and Technology, The University of Illinois at Urbana-Champaign[47]. (https://www.ks.uiuc.edu/Research/namd)

3.1.3 CHARMM force field

The name “CHARMM” stands for Chemistry at Harvard Macromolecular Mechanics (CHARMM). CHARMM is known as a set of force field parameters used for molecular dynamics simulation. It has a lot of databases of natural biomolecular structures and their force field parameters. The CHARMM force field parameters have been developed worldwide. For unknown molecules, CHARMM has the web-based graphical user interface (CHARMM-GUI) to predict the force field of that molecule. The pioneer developers are Martin Karplus and his group at Harvard University[48].

3.1.4 Packmol

Packmol is a useful software for creating the initial configurations for molecular dynamics simulation. It is used to pack molecules in space and optimize the repulsive interactions between molecules to avoid disruption of MD simulation. Packmol is software co-developed by Institute of Chemistry and Institute of Mathematics, University of Campinas and Institute of Mathematics and Statistics, University of São Paulo[49].

3.2 Methods

In this study, modifications were made to each hyaluronic acid chain to enhance its hydrophobicity. This was achieved by attaching a hydrophobic moiety or group, with the aim of facilitating the molecular assembly required to form a nanoparticle suspension in the solution. Two distinct types of hyaluronic modification were devised, known as acetylated HA and lipid-conjugated HA. Detailed information regarding the computational modeling process can be found in the subsequent section.

3.2.1 Acetylated HA nanoparticle model systems

The structure of Acetylated Hyaluronic acid (AcHA) was generated using CHARMM-GUI webserver. This involved constructing an AcHA chain model with ten HA units, single substitution of acetylation at the hydroxy group at every C6 position of N-acetyl-D-glucosamine residue was constructed through the selection of sugar type menu available in Glycan Reader & Modeler module and Input Generator module of the webserver. At the end of this step, the structure coordinates and molecular topology of the AcHA monomer were obtained. Subsequently, an assembly of 20 AcHA monomers to form a globular shape nanoparticle model (AcHA-NPs) was generated with the spherical radius of 50 Å using a packing optimization algorithm provided by PACKMOL software. This choice of 20 monomers effectively captures the nanoparticle's size, allowing for meaningful simulations of its properties and behavior without overly burdening computational resources. The

จุฬาลงกรณ์มหาวิทยาลัย
CHULALONGKORN UNIVERSITY

successfully-packed AcHA-NP model was further refined through a 20 nanosecond MD simulation in vacuum, ensuring its stability. At this step, any AcHA-NP model that failed to demonstrate stability was excluded from the subsequent step. Instead, a newly-packed AcHA-NP model was generated and subjected to MD refinement until a stable AcHA-NP model was achieved. The pre-refinement of the AcHA-NP structure was conducted to ensure that the nanoparticle model had no problematic contacts or stresses before subjecting to the simulations in the solution phase. The CHARMM36 carbohydrate and generalized CHARMM force field parameters were employed for AcHA-NP and DMSO models[50], respectively. The MD simulations were performed with the program NAMD version 2.14.

3.2.2 AcHA nanoparticle model in the DMSO-water medium

The structure and molecular topology of dimethyl sulfoxide (DMSO) were derived from the CHARMM webserver using the method as described in the previous section. DMSO is an aprotic polar solvent known for its ability to dissolve both polar and non-polar compounds. In nanoparticle preparation, it is often used to dissolve hydrophobic substances, stabilizing nanoparticles by reducing aggregation and aiding in the formation of a stable suspension. For preparing a simulation system, the pre-refined AcHA-NP model was placed in the center of the 140×140×140 $Å^3$ box and the DMSO molecules were randomly incorporated around the AcHA-NP model using PACKMOL. Then, water molecules were placed using SOLVATE module in VMD software. The number of DMSO and water molecules in each simulation system was determined based on the box size of the simulated system, along with considerations of concentration, density, and molecular weight of DMSO and water. The TIP3P[51] model was used for water molecules. Finally, the charge of the systems was neutralized by the addition of adding Na^+ and Cl^- ions to achieve overall charge neutrality. The generation of the AcHA nanoparticle model in the binary solvent mixture was executed utilizing TCL scripts in VMD.

จุฬาลงกรณ์มหาวิทยาลัย
Chulalongkorn University

To examine how DMSO impacts the AcHA assembly, MD simulations were carried out with varying concentrations of DMSO, represented as percentages by volume: 100, 80, 60, 40, 20, and 0 (referred to as DMSO100, DMSO80, DMSO60, DMSO40, DMSO20, and water, respectively). For an investigation into drug encapsulation within the nanoparticle, 15 and 30 doxorubicin (DOX) molecules (referred to as DOX15 and DOX30) were randomly positioned around the AcHA-NP within the DMSO80 system, utilizing the PACKMOL software. Additional details regarding the simulation systems are provided in **Table 3.1**. Schematic representation of the study workflow is illustrated in **Figure 3.1.**

Table 3.1 The simulated systems for MD simulation of AcHA-NP

System	Number of DMSO/water	Number of DOX	Box size ($Å^3$)	Total number of atoms
DMSO100	22,807/0	0	140x140x140	238,330
DMSO80	17,733/18,106	0	140x140x140	242,108
DMSO60	13,439/36,853	0	140x140x140	255,409
DMSO40	9,226/54,875	0	140x140x140	267,345
DMSO20	4,613/72,834	0	140x140x140	275,092
water	0/91,248	0	140x140x140	284,204
DOX15	17,733/16,101	15	140x140x140	237,113
DOX30	17,733/15,721	30	140x140x140	236,992

จุฬาลงกรณ์มหาวิทยาลัย
Chulalongkorn University

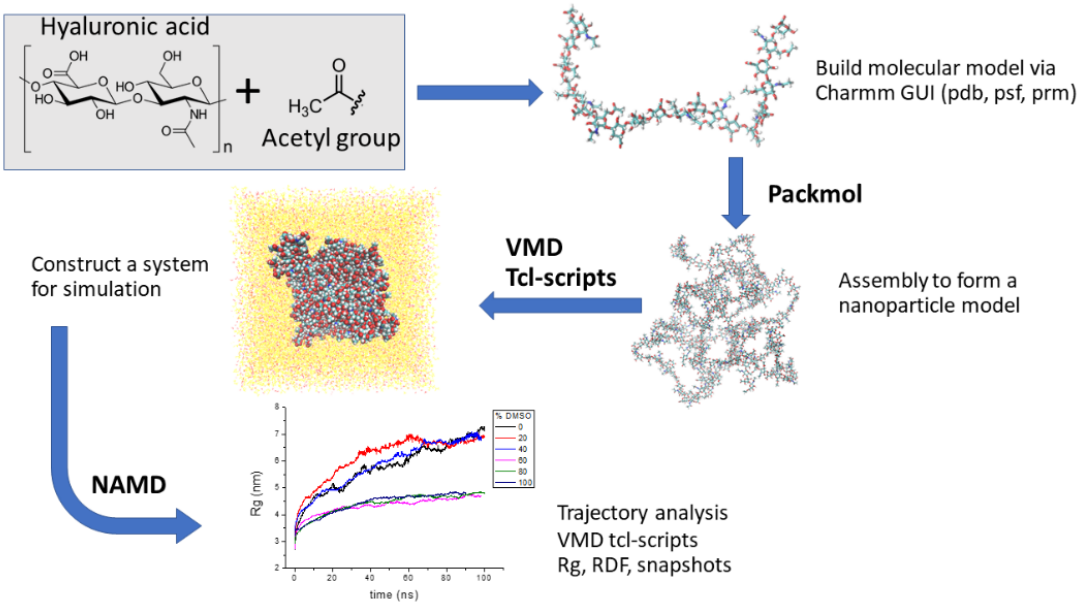

Figure 3.1 Schematic representation of the study workflow

3.2.3 Lipid-conjugated HA nanoparticle model systems

The structure of Hyaluronic Acid-Ceramide (HACe) monomer was generated using CHARMM-GUI webserver as described previously. The HACe monomer comprised four HA units and C16 ceramide (d18:1/16:0). Ceramide is a type of lipid molecule that plays a crucial role in various cellular processes, particularly in the structure and function of cell membranes. It is composed of a long-chain sphingoid base (sphingosine) and a fatty acid. At this step, the structure coordinates and molecular topology of HACe monomer was obtained through the selection of glycolipid menu available in Glycolipid Modeler module and Input Generator module of the webserver.

The PACKMOL program was utilized to construct a micelle-like structure comprising multiple HACe monomers. In this assembly, the hydrophobic ceramide portion was oriented towards the interior, while the hydrophilic hyaluronic acid segment faced outward.

3.2.4 HACe nanoparticle model in an aqueous solution

For generating a simulation system, the pre-refined HACe-NP model was placed in the center of the 160×160×160 $Å^3$ box. Then, water molecules were placed using SOLVATE module in VMD software. The TIP3P model was used for water molecules. Finally, the charge of the systems was neutralized by the addition of adding Na^+ and Cl^- ions to achieve overall charge neutrality. The generation of the HACe-NP model in the aqueous solution was executed utilizing TCL scripts in VMD.

To assess the impact of HACe monomer quantities on the micelle-like assembly, six simulation systems were established. The number of HACe monomers was varied as follows: 20, 40, 50, 60, 70, and 80 (referred to as HACe30, HACe40, HACe50, HACe60, HACe70, and HACe80, respectively). In the investigation of drug encapsulation within the nanoparticle, two doxorubicin (DOX) molecules were randomly situated inside the HACe-NP within the HACe70 system using the PACKMOL software. Additional information about the simulation systems can be found in **Table 3.2**. A schematic representation of the study workflow is provided in **Figure 3.2.**

Table 3.2 The simulated systems for MD simulation of HACe-NP

จุฬาลงกรณ์มหาวิทยาลัย
CHULALONGKORN UNIVERSITY

System	Number of waters	number of DOX	Box size ($Å^3$)	Total number of atoms
HACe30	129,856	0	160x160x160	397,436
HACe40	128,992	0	160x160x160	397,274
HACe50	128,056	0	160x160x160	396,896
HACe60	127,281	0	160x160x160	397,001
HACe70	126,426	0	160x160x160	396,866
HACe80	126,172	0	160x160x160	398,534
HACe70DOX	126,360	4	160x160x160	398,804

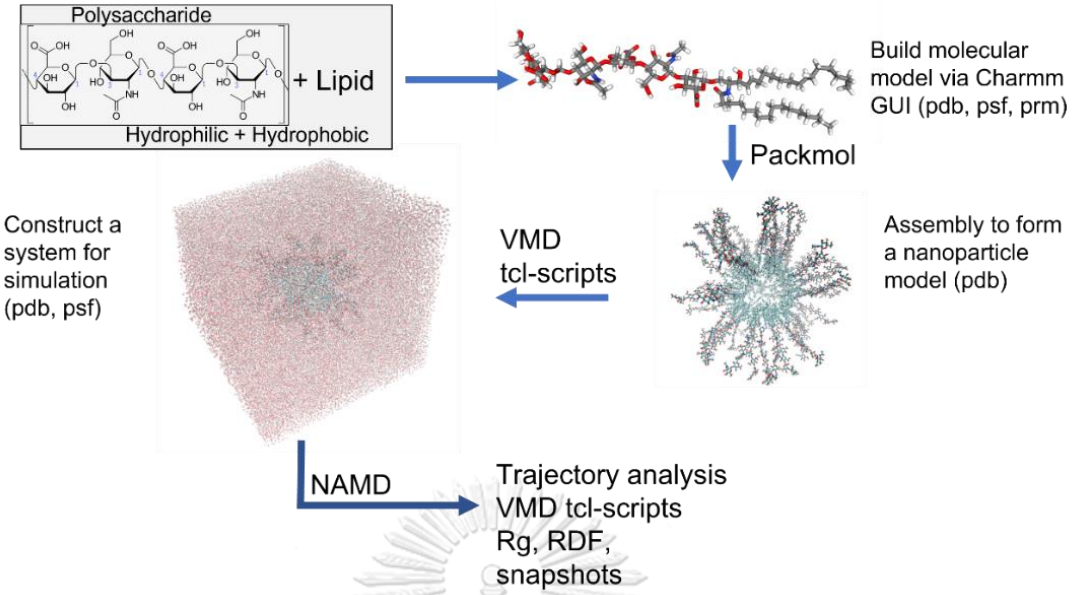

Figure 3.2 Schematic representation of the HAce-NP preparation

3.3 Molecular dynamic simulation

The NAMD2 program was employed to conduct MD simulations for all systems. The potential energy of HACe-NP was computed utilizing the generalized CHARMM force field parameters, which included glycolipid, ceramides, and spingomyelins. For the water models, TIP3P force field parameters were applied. Additionally, the CHARMM-GUI webserver was used to generate the generalized CHARMM force field parameters for the doxorubicin model. All simulation systems were run with a time step of 2 fs and performed in NPT ensemble at 1 atm and 298 K with periodic boundary conditions. Pressure was kept constant at 1 atm using the Nose´–Hoover Langevin piston method[52]. Langevin thermostat with a damping coefficient of 1 ps^{-1} was used to keep a temperature constant. Electrostatic interactions were calculated with particle mesh Ewald summation[53], including van der Waals interactions, with a cutoff distance of 12.0 Å. Bad contacts between atoms were removed by energy minimization. For trajectory storage, the MD configurations and its velocities at every 2 ps were recorded. More than 100 ns of MD simulations were performed for all AcHA-NP systems and more than 50 ns for all HACe-NP systems. MD trajectory of each system was used for the analysis.

3.4 MD trajectory analysis

All trajectory analyses were performed using TCL scripts in VMD. Unless otherwise specified, MD trajectories were extracted from the production phases of relatively long simulations for AcHA-NP and HACe-NP. Specifically, the trajectories were obtained from the last 20 ns of 100 ns simulation for AcHA-NP systems and the last 10 ns of 50 ns simulation for HACe-NP systems. This was primarily to make sure that the systems had reached thermodynamic equilibrium and that structural features extracted from the trajectory were adequately characterized with least deviation. The R_g of nanoparticle was analyzed as function of simulation time to investigate the stability and was used to estimate size of nanoparticle and R_g per chain was calculated to represent the compactness of molecules. Additionally, the number of contacts was computed to show the interactions between HA chain or DOX. Furthermore, we calculated the radial distribution function (RDF) for a particular atom (or group of atoms) in nanoparticle with solvent molecules was calculated to investigate interaction between nanoparticle and solvent molecules. All trajectory analyses were performed using TCL scripts in VMD.

จุฬาลงกรณ์มหาวิทยาลัย
Chulalongkorn University

CHAPTER 4

RESULTS AND DISCUSSION

4.1 Radius of Gyration Analysis for AcHA-NP Stability

The radius of gyration (R_g) of AcHA-NP serves as a crucial parameter for assessing the stability of AcHA assembly. As shown In **Figure 4.1**, the R_g profile is plotted against simulation time. Initially, in all systems, the R_g of AcHA-NP exhibits a rapid increase within the first 10 ns of simulation, followed by a more gradual growth rate between 10 and 100 ns. The rise in the radius of gyration indicates that the nanoparticle is undergoing a dispersion or spread out, as a result of the increased intermolecular interactions between the AcHA and solvent molecules. These interactions involve not only water but also DMSO, in addition to the inherent self-interactions among AcHA chains. Consequently, this led to the reorganization and increased flexibility of AcHA chains in the nanoparticle structure.

The R_g profile over time in the simulations exhibits two distinct behaviors, a converged low R_g and a diverged high R_g (**Figure 4.1**). This can be characterized as an expansion in the overall size or a disassembly of the AcHA chains. In the last 20ns of the simulations , the R_g values for AcHA-NP with 0%, 20% and 40% DMSO solution (water, DMSO20 and DMSO40, respectively) are notably higher (ranging between ~6.5 and ~7.5 nm) and appear to not have converged, comparison to those in 60%, 80% and 100% DMS solution (DMSO60, DMSO80 and DMSO100, respectively). The divergence of the R_g profile indicates a characteristic of a disassembly of the AcHA chains, suggesting an instability in the assembly of the AcHA-NP in the water, DMSO20 and DMSO40 systems. On the other hand, the R_g profile for DMSO60, DMSO80 and DMSO100 systems reached a plateau with average values of 4.81±0.02, 4.74±0.06, and 4.72±0.10 nm, respectively. This implies that the AcHA assembly size remains unchanged. **Figure 4.2** illustrates a representative model of the AcHA-NP taken from the MD trajectories. Interestingly, it is clearly shown that the AcHA-NP in the converged low R_g systems exhibits an amorphous structure instead of a spherical nanoparticle shape. The AcHA chains do not organize themselves into a well-defined,

จุฬาลงกรณ์มหาวิทยาลัย
Chulalongkorn University

ordered structure, but rather adopt a more disordered or irregular configuration. In case of the diverged high R_g systems, a dissociation of the AcHA chains has been observed. This leads to it a breakdown of the nanoparticle structure. Based on these MD results, it can be concluded that the AcHA nanoparticle is not stable in pure water and in DMSO-water mixtures of 20% and 40%v/v while the AcHA assembly in the binary mixture with DMSO exceeds 60%v/v. tends to form the amorphous particle.

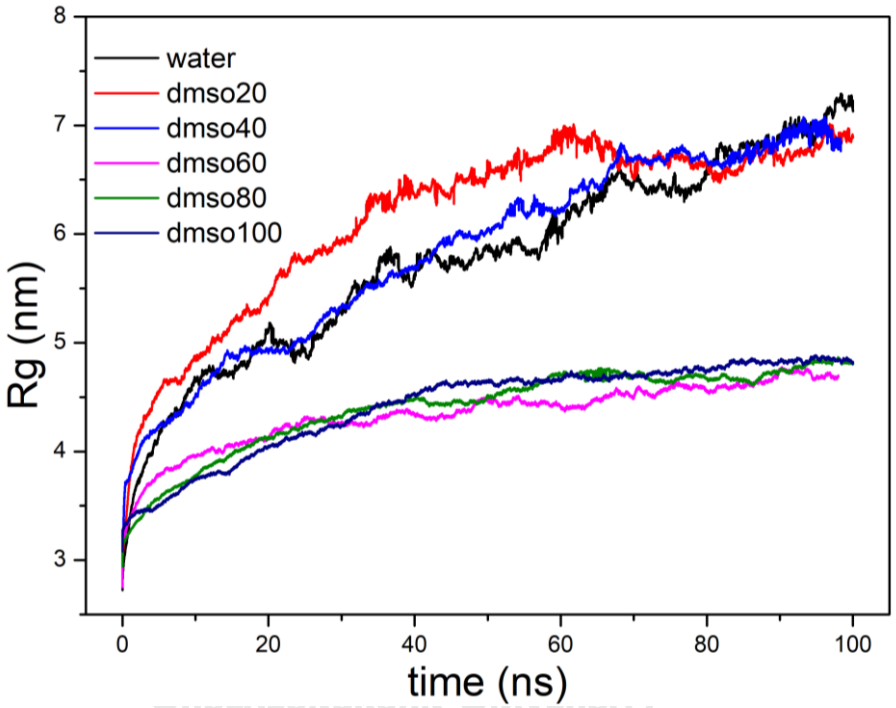

Figure 4.1 The effect of different DMSO-water solvent mixtures on the stability of the AcHA assembly.

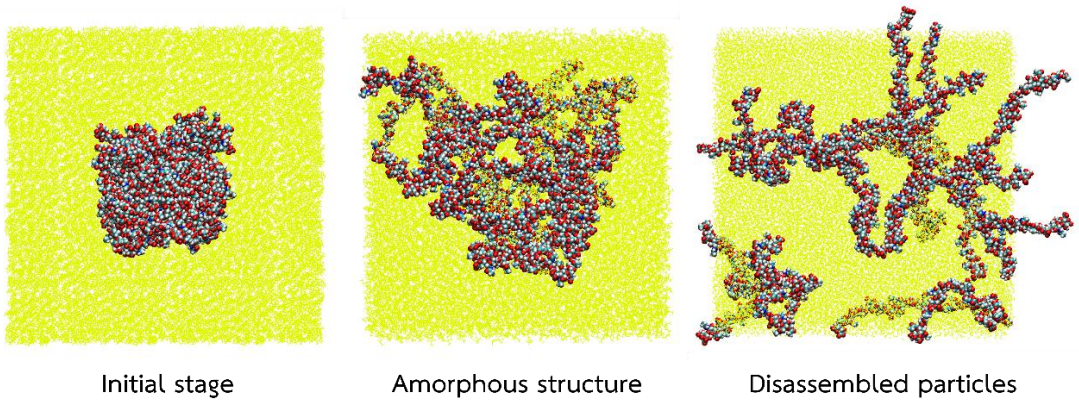

Figure 4.2 MD snapshot showing an assembly of AcHA chains into a globular shape at the initial stage (left) and amorphous structure (middle), and disassembled particles (right) at the end of the simulations

In the converged low R_g systems, there is a possibility that certain AcHA chains may detach from the structure. To obtain a more precise calculation of the Rg of the AcHA particle, it is imperative to identify which AcHA chains have separated from the structure by assessing their contact. The average number of interactions between AcHA chains can be quantified by computing the number of contacts between them. **Table 4.1** provides an overview of the average contact numbers between AcHA chains over the final 20 ns of simulation, employing a 3.0 Å cutoff. Results indicate that no AcHA chains detached in the DMSO100 system. However, in the DMSO80 and DMSO60 systems, one or two chain(s) escaped, respectively. Additionally, the average number of contacts per chain in these systems amounts to 70.8, 35.5, and 31.4 for DMSO100, DMSO80, and DMSO60, respectively.

Subsequently, a recalculated R_g was determined, excluding the AcHA chains that had detached from the nanoparticle. The new average R_g over the last 20 ns of the DMSO80 and DMSO60 systems slightly decreased from 4.74±0.06 and 4.66±0.10 to 4.26±0.04 and 4.54±0.06 nm, respectively. The radius of gyration per HA chain (R_g/N, where N is the number of AcHA chains in AcHA-NP) serves as an indicator of the overall compactness of the structure. The lower R_g/N indicates the more

compactness of structure. From **Table 4.2**, It appears that the R_g/N are 0.238, 0.237 and 0.236 nm for DMSO60, DMSO80 and DMSO100, respectively. Based on the findings pertaining to the average number of contacts and R_g/N, it can be concluded that the interaction between AcHA chains and compactness of AcHA-NP structure diminishes with increasing solvent polarity.

Table 4.1 Average number of contacts between AcHA chains with 3.0 Å cutoff

HA chain ID	The average number of contacts		
	DMSO60	DMSO80	DMSO100
A	42.4±11.7	49.2±10.7	143.3±6.9
B	73.3±11.1	159.4±14.0	143.3±20.4
C	142.9±34.8	84.8±18.8	196.8±25.4
D	23.5±8.4	40.5±12.6	238.2±15.5
E	65.6±16.9	86.3±22.5	221.5±21.6
F	18.0±5.4	22.6±6.7	117.6±10.5
G	56.1±15.3	146.2±24.0	128.9±8.2
H	0±0.0	0±0.0	18.8±5.8
I	14.8±6.0	18.0±6.3	25.7±5.3
J	53.5±14.0	70.3±15.0	199.6±17.7
K	65.2±13.0	73.6±14.7	121.8±14.4
L	128.6±25.5	141.3±18.5	257.3±23.5
M	62.3±14.6	12.5±4.2	120.3±9.9
N	31.7±15.5	51.7±9.6	109.0±13.9
O	51.5±19.4	42.2±18.0	99.3±12.5
P	49.0±11.9	63.2±14.9	78.4±10.8
Q	37.3±13.2	36.3±19.0	126.2±11.9
R	142.9±34.8	157.1±26	220.7±17.7
S	73.1±22.3	26.9±12.6	165.8±16.4
T	62.2±16.1	0±0	101.1±11.5

จุฬาลงกรณ์มหาวิทยาลัย
Chulalongkorn University

Table 4.2 Calculation of radius of gyration per HA chain

Variable	DMSO60	DMSO80	DMSO100
Number of HA chains (N)	19	18	20
Radius of gyration (R_g)	4.54	4.26	4.72
Radius of gyration per HA chain (R_g/N)	0.238	0.237	0.236

4.2 Interaction between AcHA-NPs and solvent

The hydroxyl group within AcHA exhibits an affinity for forming hydrogen bonds with water molecules. This interaction was elucidated through the calculation of the radial pair distribution function (g(r)) between AcHA and water molecules, utilizing trajectory data from the final 20 ns of simulation. The g(r) plots show the probability of finding a pair of atoms/groups of atoms at a given distance from each other. **Figure 4.3a** illustrates the resulting g(r) plot, revealing the density distribution of oxygen and hydrogen atoms of water in relation to the hydroxyl group of AcHA. The initial sharp peak denotes the first hydration shell, signifying a high likelihood of hydrogen bond formation between the hydroxyl group of AcHA and neighboring water molecules. Notably, the consistent location of the first peak in both plots indicates that water molecules serve not only as hydrogen bond acceptors but also as donors. Furthermore, an exploration of the interaction between AcHA and DMSO molecules was conducted by plotting g(r) between AcHA and the carbon and oxygen atoms of DMSO (**Figure 4.3b**). This plot delineates the first sharp peak of the oxygen atom, positioning it closer to the y-axis than the carbon atom. This suggests a propensity for AcHA to interact with the oxygen atom of DMSO rather than its carbon counterpart.

Additionally, an investigation into the interactions between the oxygen atom of DMSO and various elements within AcHA was undertaken. **Figure 4c** displays g(r) between the oxygen atom of DMSO and elements in AcHA, encompassing hydrogen, carbon, nitrogen, and oxygen. The peak closest to the y-axis corresponds to the hydrogen atom. Subsequently, g(r) was plotted between the oxygen atom of DMSO and distinct types of hydrogen in HA, including hydrogen on the C6 atom of the sugar

ring (HC_6), tertiary hydrogen (H3°), primary hydrogen (H1°), amide hydrogen (H_N), and hydroxy hydrogen (H_O) (**Figure 4d**). This plot reveals peaks associated with the amide hydrogen and hydroxy hydrogen, positioned closest to the y-axis. Based on these g(r) plots, it can be concluded that the oxygen atom of DMSO exhibits a preference for acting as the hydrogen bond acceptor from the amide group and the hydroxyl group of AcHA.

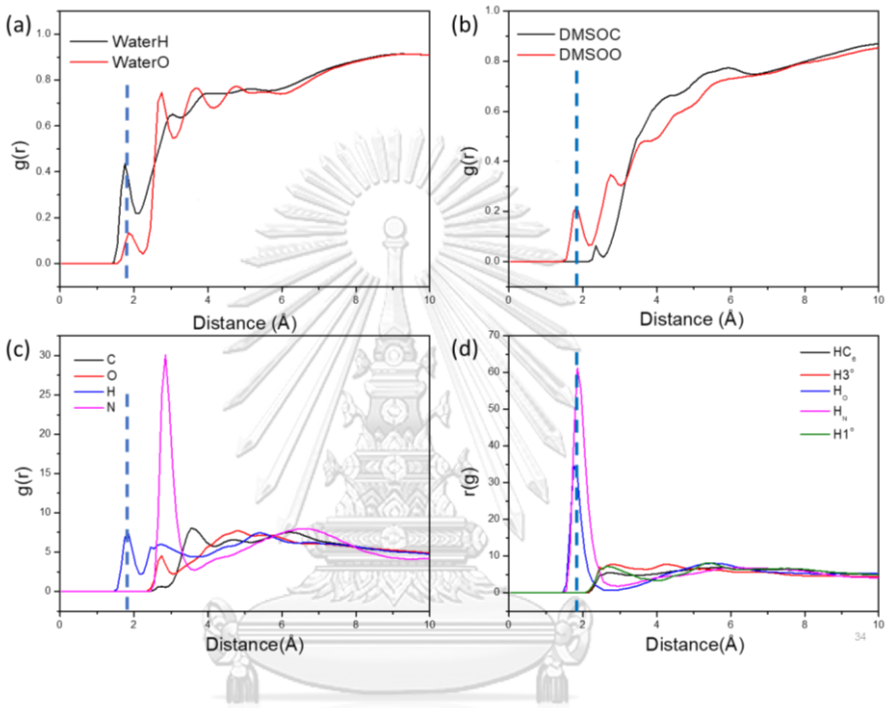

Figure 4.3 The interactions between AcHA and the solvent components. (a) The g(r) plot between the hydroxyl group of AcHA and the hydrogen and oxygen atoms of water. (b) The g(r) between the HA and the carbon and oxygen atoms of DMSO. (c) The g(r) between the oxygen atom of DMSO and the different elements in HA. (d) The g(r) between the oxygen atom of DMSO and the various types of hydrogen atoms in HA.

จุฬาลงกรณ์มหาวิทยาลัย
Chulalongkorn University

4.3 DOX loading capability of AcHA-NPs

For the investigation of DOX loading within AcHA-NP, the choice of DMSO at 80%v/v was pivotal for the simulations. The stability of DOX-loaded AcHA-NP was assessed by monitoring the R_g over time. In the DOX15 system, the R_g profile stabilized, signifying the robustness of the AcHA-NP upon DOX integration (Figure 4.4).

The average R_g over the final 20 ns of simulation for the DOX15 system was 3.79±0.02 nm.

Comparatively, the R_g value in the DOX15 system was notably lower than that in the DMSO80 system without DOX. This reduction in R_g indicates a smaller size of AcHA-NP when DOX is present. The introduction of DOX facilitated the self-assembly of AcHA, leveraging its hydrophobic properties. In the absence of DOX, hydrophobic interactions were limited to the acetyl group. However, with the inclusion of DOX, these interactions intensified between DOX and the acetyl group of AcHA, enhancing the stability of AcHA-NP[15].

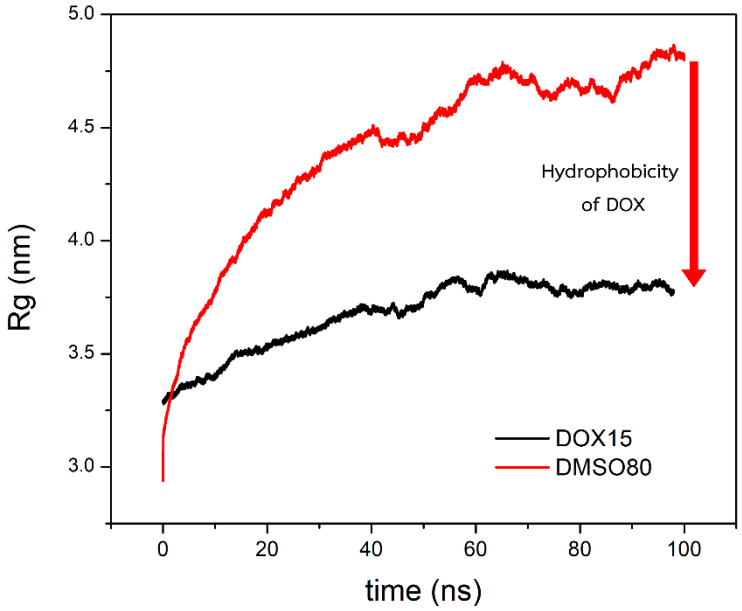

CHULALONGKORN UNIVERSITY

Figure 4.4 The effect of DOX drug on the AcHA-NP size. The R_g profile of the AcHA-NP was calculated from 100 ns simulations in the presence and absence of the DOXdrug. The presence of DOX drug reduced the R_g values of the AcHA-NP, indicating a more compact structure.

To assess the potential of AcHA-NPs as drug carriers, an evaluation of their DOX-loading capacity was imperative. This was achieved by quantifying the number of adsorbed DOX molecules, defined as those with a center of mass within 7 Å of AcHA-NPs. **Figure 4.6** illustrates the progression of adsorbed DOX over the simulation duration. Initially, there is a decline in the number of adsorbed DOX, which

eventually stabilizes, indicating an equilibrium state. This decrease in adsorbed DOX can be attributed to the solvation of DOX, involving interactions with solvent molecules. For the DOX15 system, the average number of adsorbed DOX over the last 20 ns of simulation was 3.9±0.9 molecules. To ascertain the maximum capacity for adsorbed DOX by AcHA-NPs, the concentration of DOX was augmented, increasing the initial number of DOX molecules from 15 to 30. The resulting DOX30 system showed an average of 4.6±1.1 adsorbed DOX molecules, a statistically insignificant deviation from the DOX15 system. Given that both systems exhibited an adsorbed DOX count of approximately 4 molecules, the equilibrium number of adsorbed DOX molecules on the AcHA-NP surface is independent of the initial concentration of DOX in the solvent. This suggests that the adsorption process is limited by the availability of binding sites on the AcHA-NP surface, as shows **Figure 4.5**, rather than by the diffusion of DOX molecules from the bulk solvent. This also implies that the AcHA-NP has a high affinity for DOX drug and can be used as a drug carrier.

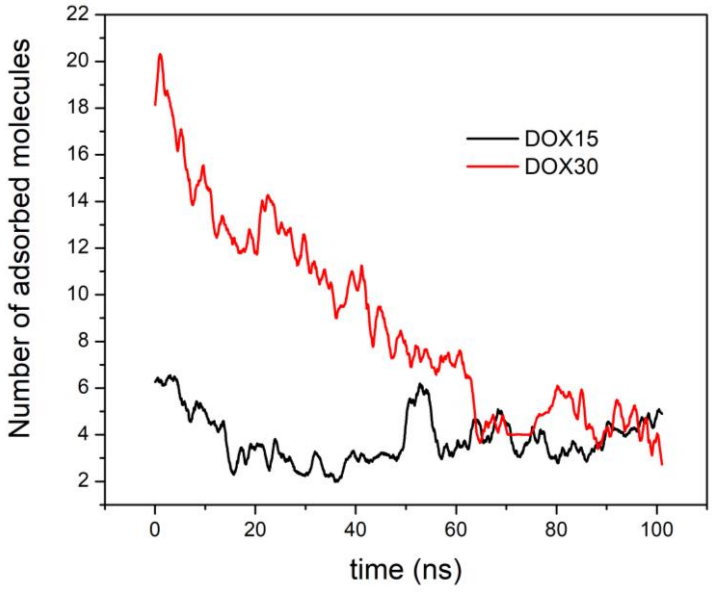

Figure 4.5 The adsorption of DOX drug on the AcHA-NP surface. The number of adsorbed DOX molecules was counted as a function of time during 100 ns simulations with two different concentrations of DOX: 15 and 30 molecules. As the system approaching an equilibrium, the number of adsorbed DOX molecules on the AcHA surface approaches a similar quantity value for both the DOX30 system and the DOX15 system

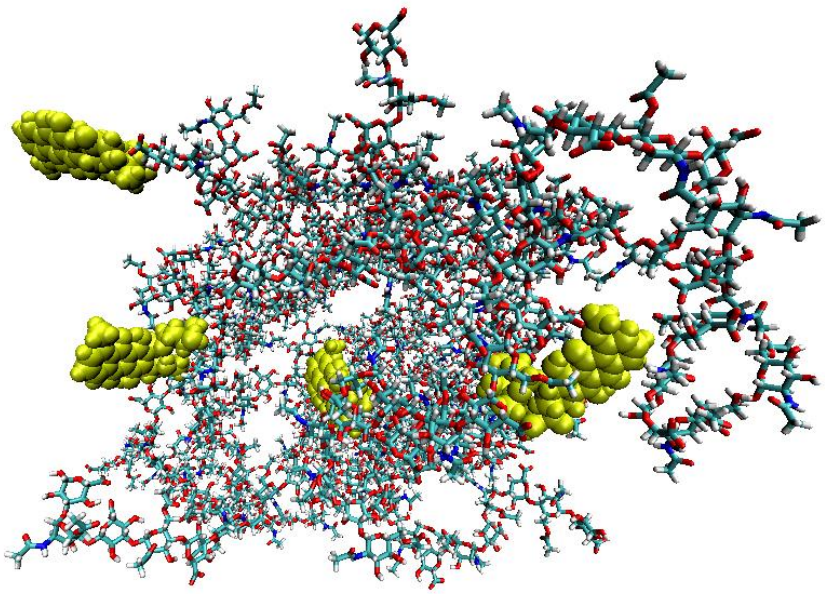

Figure 4.6 MD snapshot showing the adsorption of DOX drug (yellow) on the AcHA-NP surface.

4.4 Stability of HACe-NPs

For HAce-NP systems, the evaluation of the HACe assembly's stability is conducted using the radius of gyration (R_g). **Figure 4.7** illustrates the Rg profile of HACe-NP over time. In the HACe70 and HACe80 systems, the R_g demonstrates a decreasing trend, stabilizing towards the end of the simulation. This decline in R_g value suggests the assembly of HACe facilitated by hydrophobic interactions within the nonpolar tails. In contrast, for HACe30, HACe40, HACe50, and HACe60 systems, the R_g shows an increasing trend over time, surpassing that of HACe70 and HACe80 systems. This indicates the instability of HACe30, HACe40, HACe50, and HACe60 systems. Specifically, the average R_g for the last 20 ns of simulation in HACe70 and HACe80 systems is 3.51±0.02 and 3.61±0.02 nm, respectively. **Figure 4.8** presents various snapshots of HACe-NP configurations, including both stable and unstable nanoparticle models, alongside the initial structure. The stable nanoparticle model shows a well-defined structure where the hydrophobic part is within the inner core and the polar part is exposed to the solvent. Based on these results, it can be

concluded that a stable HACe-NP can be constructed using a combination of HACe 70 and 80 molecules.

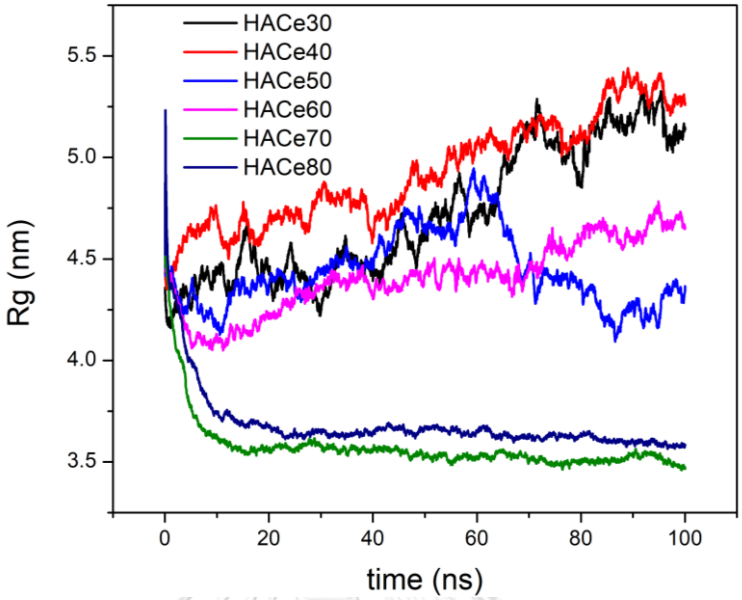

Figure 4.7 The effect of different numbers of HACe molecules on the HACe-NP size. The R_g profile of the HACe-NP was calculated from 100 ns simulations with varying numbers of HACe molecules in the system. The R_g values decreased as the number of HACe molecules increased, indicating a more compact and stable structure of the HACe-NP.

จุฬาลงกรณ์มหาวิทยาลัย

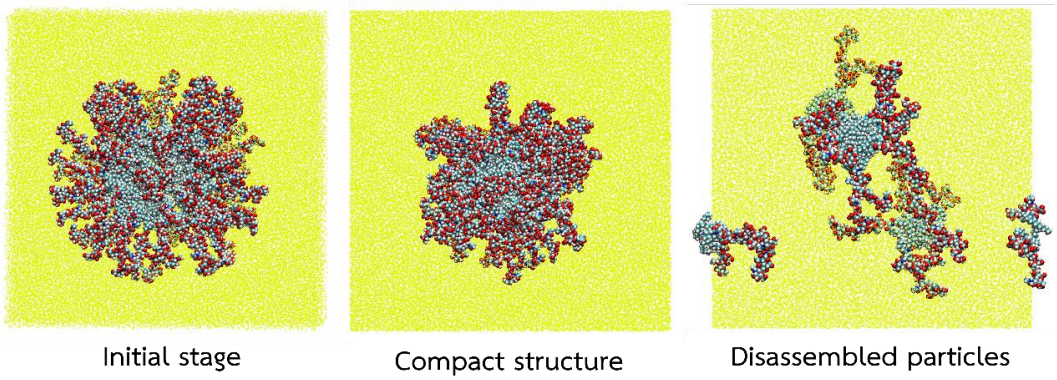

Figure 4.8 The structural stability of the HACe-NP. An assembly of HACe chains into a micelles-like structure at the initial stage (left) and compact structure (middle), and disassembled particles (right) at the end of the simulations.

4.5 Interaction between HACe-NPs and solvent

For an in-depth exploration of the interaction between HACe-NP and the solvent, the radial distribution function g(r) is computed for both HACe70 and HACe80 systems. This calculation involves assessing the correlation between the center of mass of HACe-NP and water molecules. As depicted in **Figure 4.9**, when the g(r) value is in close proximity to the center of mass and equals 0, it signifies the absence of water molecules within the hydrophobic shell of HACe-NP. This means that the HACe molecules form a tight and impermeable coating on the HACe-NP surface, preventing water from penetrating into the core. This could enhance the stability and drug-loading capacity of the HACe-NP.

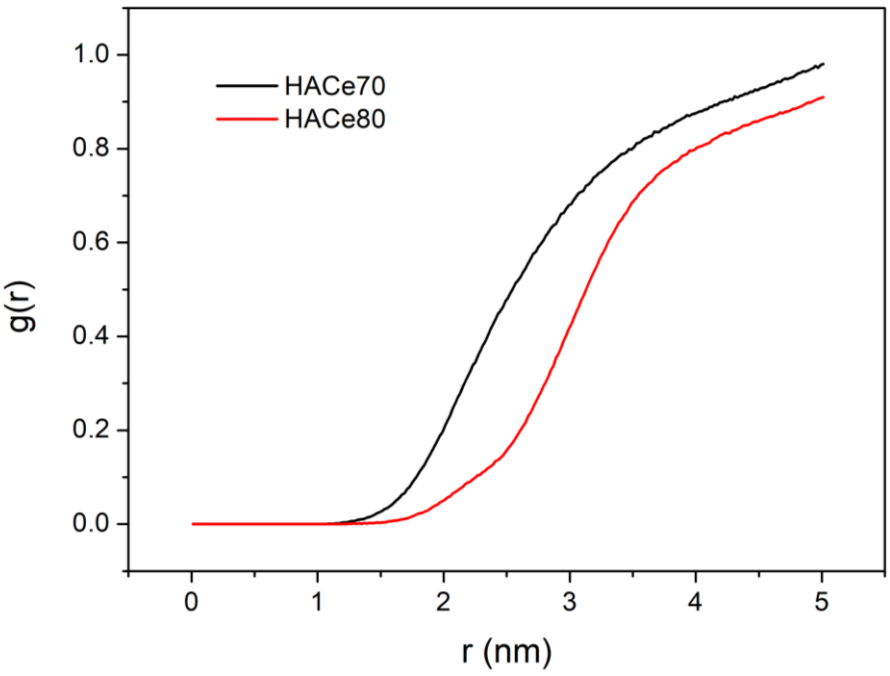

Figure 4.9 The g(r) plot shows the probability of finding a water molecule at a given distance from the center of mass of the HACe-NP. The g(r) was calculated from 100 ns simulations with different numbers of HACe molecules in the system. The absence of a peak in the g(r) plot within the first 10Å suggests that there is no water present in the inner or hydrophobic core of the HACe nanoparticle.

4.6 Encapsulation of DOX by HACe-NP

To investigate HACe-NPs' potential as carriers for DOX, an MD simulation of the HACe-NP system incorporating DOX was performed. The stability of HACe-NP was assessed by plotting its R_g over time, as illustrated in **Figure 4.10.** The profile of R_g for HACe-NP exhibited a rapid decrease in the initial 10 ns, followed by a sustained stability, indicating the stability of HACe-NP in the presence of the DOX drug.

Additionally, distances were calculated: one between the center of mass of HACe-NP and the oxygen atom labeled O1, which links the hydrophobic tail and hydrophilic head, providing an estimate for the radius of the hydrophobic shell of HACe-NP. The other distance was between the center of mass of HACe-NP and the center of mass of each DOX molecule. As shown in **Figure 4.11**, the behavior of the average distance between the center of mass of HACe-NP and the oxygen atom labeled O1 paralleled the R_g plot, with a rapid decrease in the initial 10 ns followed by stabilization. The calculated average distance during the last 10 ns of simulation was 2.7±0.01 nm, which can serve as the radius of the hydrophobic shell at equilibrium. By analyzing the results of the distances between the center of mass of HACe-NP and each DOX molecule, one can approximate the position of DOX within HACe-NP. Comparing this information with the radius of the hydrophobic core, it can be deduced that all four DOX molecules are situated at the surface of the hydrophobic shell of HACe-NP as shown in **Figure 4.12**. Based on the MD results, it can be concluded that HACe-NP has the potential to serve as a carrier for DOX, with DOX predominantly located near the surface of the hydrophobic shell.

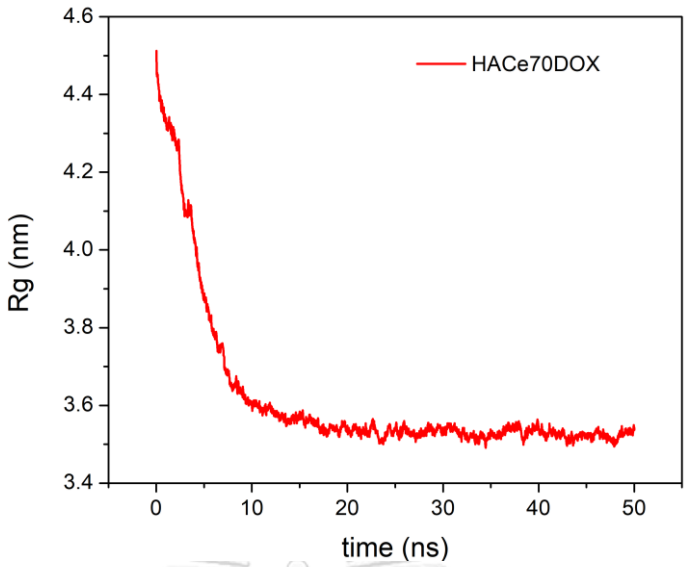

Figure 4.10 The effect of DOX drug on the HACe-NP size and stability.

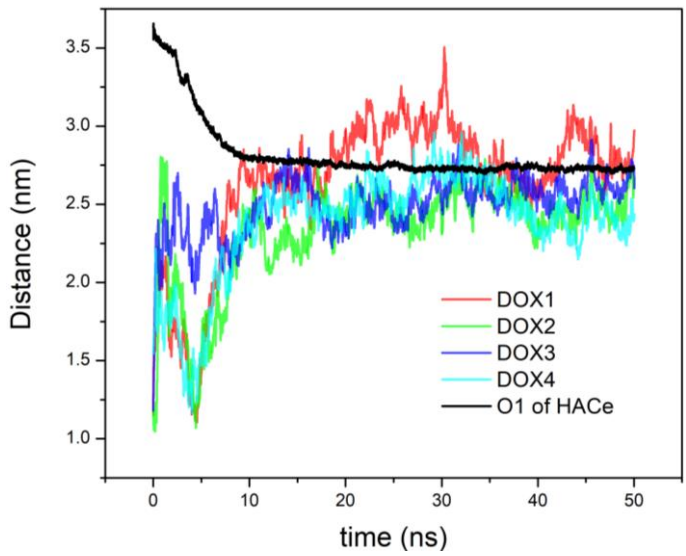

Figure 4.11 The encapsulation of the DOX drug on the HACe-NP surface. The distance between the center of mass of the HACe-NP and the center of mass of each DOX molecule (DOX1, DOX2, DOX3 and DOX4) in the system was calculated from 50 ns simulations. The distance between the center of mass of the HACe-NP and the oxygen atom O1 of HACe was also calculated to estimate the size of the inner core of the nanoparticle model. The distance values indicate how close the DOX drug to the inner hydrophobic core of the HACe-NP.

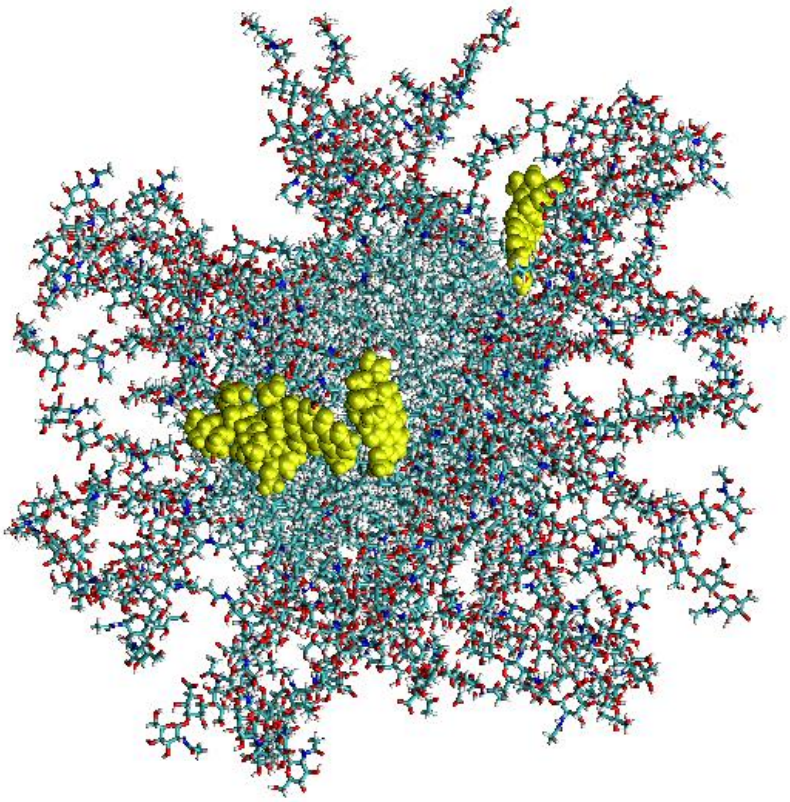

Figure 4.12 MD snapshot showing the encapsulation of DOX drug (yellow) on the AcHA-NP surface.

จุฬาลงกรณ์มหาวิทยาลัย
Chulalongkorn University

CHAPTER 5

CONCLUSIONS

The stability and drug loading capacity of chemically-modified hyaluronic acid nanoparticles (HANPs) were investigated using molecular dynamics simulations. Two types of HANPs were considered: acetylated hyaluronic acid nanoparticles (AcHA-NPs) and ceramide-conjugated hyaluronic acid nanoparticles (HACe-NPs). Based on the MD results, the study can be concluded as follows:

5.1 Acetylated hyaluronic acid nanoparticles (AcHA-NP)

The stability of AcHA-NP assembly was assessed in a DMSO-water mixture at various concentrations, including 0%, 20%, 40%, 60%, 80% and 100% DMSO by volume. MD results revealed a disassembly of the AcHA-NP in pure water and in DMSO-water mixtures of 20% and 40% by volume. On the other hand, no significant disintegration of the AcHA-NP was observed in solutions containing DMSO at 60%, 80% and 100% by volume, indicating that higher DMSO concentrations enhance the stability of AcHA-NP. However, it was noted that the stable AcHA-NP adopts an amorphous structure rather than a well-organized one. This can be attributed to the ability of DMSO, an aprotic solvent, to reduce solvent polarity, thereby increasing interactions between AcHA chains (solute-solute interactions). Consequently, DMSO plays a pivotal role in sustaining the stability of the AcHA nanoparticles, as it hinders interactions between AcHA molecules and water through hydrogen bonding.

จุฬาลงกรณ์มหาวิทยาลัย
Chulalongkorn University

5.2 Drug-loading capability of AcHA-NP

The MD study involving the incorporation of doxorubicin into AcHA-NP yielded valuable insights into the drug adsorption onto the nanoparticle. MD results indicated that the introduction of the drug did not significantly reduce the stability of

the AcHA assembly. Instead, the drug was sustained onto the surface of the AcHA-NP through hydrophobic interactions between the acetyl groups of the AcHA-NP and doxorubicin, as well as solvent repulsion. Additionally, the nanoparticle exhibited a more compact structure, suggesting its potential as a drug carrier for the drug. This results are consistent with the drug loading study of the AcHA-NP[15]. It is important to note that due to the amorphous structure of the nanoparticle, there is no specific binding site for the drug. Moreover, with an increase in drug concentration, it became evident that AcHA-NP maintained a consistent drug-loading capacity for a hydrophobic drug, like doxorubicin.

5.3 Ceramide-conjugated hyaluronic acid nanoparticle (HACe-NP)

The stability of the ceramide-conjugated-hyaluronic acid nanoparticle assembly in an aqueous solution was assessed by manipulating the size and number of HACe chains to create a representative model of HACe-nanoparticle. This investigation demonstrated that by achieving an appropriate balance between the size and quantity of HACe chains, a stable assembly of HACe-NP could be successfully achieved in the aqueous solvent. The resulting HACe-NP assembly exhibited a well-organized micelle-like structure, with hydrophobic regions oriented inward and polar regions exposed to the aqueous environment. The inner core of the HACe-NP displayed a notable hydrophobic nature, as evidenced by the absence of water molecules in this region.

จุฬาลงกรณ์มหาวิทยาลัย
CHULALONGKORN UNIVERSITY

5.4 Drug-loading capability of HACe-NP

To assess the potential of HACe-NPs as carriers for doxorubicin, an MD simulation was conducted incorporating the drug into the HACe-NP system. The results demonstrated successful binding of the drug to the HACe-NP, and the presence of doxorubicin did not destabilize the HACe-NP assembly. Specifically, doxorubicin molecules were observed to cluster around the ceramide fragment of the HACe-NP. Based on these findings, it can be inferred that HACe-NP holds promise

as a carrier for doxorubicin, with the drug predominantly located near the surface of the nanoparticle's hydrophobic region.

จุฬาลงกรณ์มหาวิทยาลัย
Chulalongkorn University

REFERENCES

1 Sung, H.; Ferlay, J.; Siegel, R. L.; Laversanne, M.; Soerjomataram, I.; Jemal, A.; Bray, F. Global cancer statistics 2020: GLOBOCAN estimates of incidence and mortality worldwide for 36 cancers in 185 countries. *CA: A Cancer Journal For Clinicians* **2021**, *71* (3), 209-249.

2 Moo, T.-A.; Sanford, R.; Dang, C.; Morrow, M. Overview of breast cancer therapy. *PET Clinics* **2018**, *13* (3), 339-354.

3 Marin, J. J.; Romero, M. R.; Blazquez, A. G.; Herraez, E.; Keck, E.; Briz, O. Importance and limitations of chemotherapy among the available treatments for gastrointestinal tumours. *Anti-Cancer Agents in Medicinal Chemistry (Formerly Current Medicinal Chemistry-Anti-Cancer Agents)* **2009**, *9* (2), 162-184.

4 Gutteridge, W. E. Existing chemotherapy and its limitations. *British Medical Bulletin* **1985**, *41* (2), 162-168.

5 Sawyers, C. Targeted cancer therapy. *Nature* **2004**, *432* (7015), 294-297.

6 Damodharan, J. Nanomaterials in medicine–An overview. *Materials Today: Proceedings* **2021**, *37*, 383-385.

7 Yaqoob, A. A.; Ahmad, H.; Parveen, T.; Ahmad, A.; Oves, M.; Ismail, I. M.; Qari, H. A.; Umar, K.; Mohamad Ibrahim, M. N. Recent advances in metal decorated nanomaterials and their various biological applications: A review. *Frontiers in Chemistry* **2020**, *8*, 341.

8 Shimon, M. B.; Shapira, S.; Seni, J.; Arber, N. The Big Potential of Small Particles: Lipid-Based Nanoparticles and Exosomes in Vaccination. *Vaccines* **2022**, *10* (7), 1119.

9 Mehnert, W.; Mäder, K. Solid lipid nanoparticles: production, characterization and applications. *Advanced Drug Delivery Reviews* **2012**, *64*, 83-101.

10 Chauhan, A. S. Dendrimers for drug delivery. *Molecules* **2018**, *23* (4), 938.

11 Bharti, C.; Nagaich, U.; Pal, A. K.; Gulati, N. Mesoporous silica nanoparticles in target drug delivery system: A review. *International Journal of Pharmaceutical Investigation* **2015**, *5* (3), 124.

จุฬาลงกรณ์มหาวิทยาลัย
Chulalongkorn University

12 Abdolahinia, E. D.; Barati, G.; Ranjbar-Navazi, Z.; Kadkhoda, J.; Islami, M.; Hashemzadeh, N.; Dizaj, S. M.; Sharifi, S. Application of nanogels as drug delivery systems in multicellular spheroid tumor model. *Journal of Drug Delivery Science and Technology* **2022**, *68*, 103109.

13 Bose, A.; Roy Burman, D.; Sikdar, B.; Patra, P. Nanomicelles: Types, properties and applications in drug delivery. *IET Nanobiotechnology* **2021**, *15* (1), 19-27.

14 Begines, B.; Ortiz, T.; Pérez-Aranda, M.; Martínez, G.; Merinero, M.; Argüelles-Arias, F.; Alcudia, A. Polymeric nanoparticles for drug delivery: Recent developments and future prospects. *Nanomaterials* **2020**, *10* (7), 1403.

15 Park, W.; sub Kim, K.; Bae, B.-c.; Kim, Y.-H.; Na, K. Cancer cell specific targeting of nanogels from acetylated hyaluronic acid with low molecular weight. *European Journal of Pharmaceutical Sciences* **2010**, *40* (4), 367-375.

16 Kim, K.; Choi, H.; Choi, E. S.; Park, M.-H.; Ryu, J.-H. Hyaluronic acid-coated nanomedicine for targeted cancer therapy. *Pharmaceutics* **2019**, *11* (7), 301.

17 Fraser, J. R. E.; Laurent, T. C.; Laurent, U. Hyaluronan: its nature, distribution, functions and turnover. *Journal of Internal Medicine* **1997**, *242* (1), 27-33.

18 Necas, J.; Bartosikova, L.; Brauner, P.; Kolar, J. Hyaluronic acid (hyaluronan): a review. *Veterinarni Medicina* **2008**, *53* (8), 397-411.

19 Jiang, D.; Liang, J.; Noble, P. W. Hyaluronan in tissue injury and repair. *Annu. Rev. Cell Dev. Biol.* **2007**, *23*, 435-461.

20 Aruffo, A.; Stamenkovic, I.; Melnick, M.; Underhill, C. B.; Seed, B. CD44 is the principal cell surface receptor for hyaluronate. *Cell* **1990**, *61* (7), 1303-1313.

21 Schiffelers, R. M.; Ansari, A.; Xu, J.; Zhou, Q.; Tang, Q.; Storm, G.; Molema, G.; Lu, P. Y.; Scaria, P. V.; Woodle, M. C. Cancer siRNA therapy by tumor selective delivery with ligand-targeted sterically stabilized nanoparticle. *Nucleic Acids Research* **2004**, *32* (19), e149-e149.

22 Lee, H.; Ahn, C. H.; Park, T. G. Poly [lactic-co-(glycolic acid)]-grafted hyaluronic acid copolymer micelle nanoparticles for target-specific delivery of doxorubicin. *Macromolecular Bioscience* **2009**, *9* (4), 336-342.

23 Arcamone, F.; Cassinelli, G.; Fantini, G.; Grein, A.; Orezzi, P.; Pol, C.; Spalla, C.

จุฬาลงกรณ์มหาวิทยาลัย
Chulalongkorn University

Adriamycin, 14-Hydroxydaunomycin, a new antitumor antibiotic from S. peucetius var. caesius. *Biotechnology and Bioengineering* **2000**, *67* (6), 704-713.

24 Thorn, C. F.; Oshiro, C.; Marsh, S.; Hernandez-Boussard, T.; McLeod, H.; Klein, T. E.; Altman, R. B. Doxorubicin pathways: pharmacodynamics and adverse effects. *Pharmacogenetics and Genomics* **2011**, *21* (7), 440.

25 Atkins, E.; Meader, D.; Scott, J. Model for hyaluronic acid incorporating four intramolecular hydrogen bonds. *International Journal of Biological Macromolecules* **1980**, *2* (5), 318-319.

26 Holmbeck, S. M.; Petillo, P. A.; Lerner, L. E. The solution conformation of hyaluronan: a combined NMR and molecular dynamics study. *Biochemistry* **1994**, *33* (47), 14246-14255.

27 Almond, A.; Sheehan, J. K.; Brass, A. Molecular dynamics simulations of the two disaccharides of hyaluronan in aqueous solution. *Glycobiology* **1997**, *7* (5), 597-604.

28 Almond, A.; Brass, A.; Sheehan, J. Deducing polymeric structure from aqueous molecular dynamics simulations of oligosaccharides: predictions from simulations of hyaluronan tetrasaccharides compared with hydrodynamic and X-ray fibre diffraction data. *Journal of Molecular Biology* **1998**, *284* (5), 1425-1437.

29 Donati, A.; Magnani, A.; Bonechi, C.; Barbucci, R.; Rossi, C. Solution structure of hyaluronic acid oligomers by experimental and theoretical NMR, and molecular dynamics simulation. *Biopolymers: Original Research on Biomolecules* **2001**, *59* (6), 434-445.

30 Bayraktar, H.; Akal, E.; Sarper, O.; Varnali, T. Modeling glycosaminoglycans—hyaluronan, chondroitin, chondroitin sulfate A, chondroitin sulfate C and keratan sulfate. *Journal of Molecular Structure: THEOCHEM* **2004**, *683* (1-3), 121-132.

31 Furlan, S.; La Penna, G.; Perico, A.; Cesàro, A. Hyaluronan chain conformation and dynamics. *Carbohydrate Research* **2005**, *340* (5), 959-970.

32 Pogány, P.; Kovács, A. Conformational properties of the disaccharide building units of hyaluronan. *Carbohydrate Research* **2009**, *344* (13), 1745-1752.

จุฬาลงกรณ์มหาวิทยาลัย
Chulalongkorn University

33 Gargiulo, V.; Morando, M. A.; Silipo, A.; Nurisso, A.; Pérez, S.; Imberty, A.; Cañada, F. J.; Parrilli, M.; Jimenez-Barbero, J.; De Castro, C. Insights on the conformational properties of hyaluronic acid by using NMR residual dipolar couplings and MD simulations. *Glycobiology* **2010**, *20* (10), 1208-1216.

34 Payne, W. M.; Svechkarev, D.; Kyrychenko, A.; Mohs, A. M. The role of hydrophobic modification on hyaluronic acid dynamics and self-assembly. *Carbohydrate Polymers* **2018**, *182*, 132-141.

35 Taweechat, P.; Pandey, R. B.; Sompornpisut, P. Conformation, flexibility and hydration of hyaluronic acid by molecular dynamics simulations. *Carbohydrate research* **2020**, *493*, 108026.

36 Liang, L.; Shen, J.-W.; Wang, Q. Molecular dynamics study on DNA nanotubes as drug delivery vehicle for anticancer drugs. *Colloids and Surfaces B: Biointerfaces* **2017**, *153*, 168-173.

37 Leach, A. R. *Molecular modelling: principles and applications*; Pearson education, 2001.

38 González, M. A. Force fields and molecular dynamics simulations. *École thématique de la Société Française de la Neutronique* **2011**, *12*, 169-200.

39 Monticelli, L.; Tieleman, D. P. Force fields for classical molecular dynamics. *Biomolecular Simulations: Methods and Protocols* **2013**, 197-213.

40 Allen, M.; Tildesley, D. Computer Simulation of Liquids Oxford University Press Oxford 385. **1987**.

41 Hug, S. Classical molecular dynamics in a nutshell. *Biomolecular Simulations: Methods and Protocols* **2013**, 127-152.

42 Cramer, C. J. *Essentials of computational chemistry: theories and models*; John Wiley & Sons, 2013.

43 Lindahl, E.; Hess, B.; Van Der Spoel, D. GROMACS 3.0: a package for molecular simulation and trajectory analysis. *Molecular modeling annual* **2001**, *7*, 306-317.

44 van der Spoel, D.; Lindahl, E.; Hess, B.; Van Buuren, A.; Apol, E.; Meulenhoff, P.; Tieleman, D.; Sijbers, A.; Feenstra, K.; van Drunen, R. GROMACS user manual version 3.2. *Nijenborgh* **2004**, *4*, 9747.

45 Humphrey, W.; Dalke, A.; Schulten, K. VMD: visual molecular dynamics. *Journal*

จุฬาลงกรณ์มหาวิทยาลัย
Chulalongkorn University

of Molecular Graphics **1996**, *14* (1), 33-38.

46 Hsin, J.; Arkhipov, A.; Yin, Y.; Stone, J. E.; Schulten, K. Using VMD: an introductory tutorial. *Current Protocols in Bioinformatics* **2008**, *24* (1), 5.7. 1-5.7. 48.

47 Kalé, L.; Skeel, R.; Bhandarkar, M.; Brunner, R.; Gursoy, A.; Krawetz, N.; Phillips, J.; Shinozaki, A.; Varadarajan, K.; Schulten, K. NAMD2: greater scalability for parallel molecular dynamics. *Journal of Computational Physics* **1999**, *151* (1), 283-312.

48 MacKerell Jr, A. D.; Brooks, B.; Brooks III, C. L.; Nilsson, L.; Roux, B.; Won, Y.; Karplus, M. CHARMM: the energy function and its parameterization. *Encyclopedia of Computational Chemistry* **2002**, *1*.

49 Martínez, L.; Andrade, R.; Birgin, E. G.; Martínez, J. M. PACKMOL: A package for building initial configurations for molecular dynamics simulations. *Journal of Computational Chemistry* **2009**, *30* (13), 2157-2164.

50 Brooks, B. R.; Brooks III, C. L.; Mackerell Jr, A. D.; Nilsson, L.; Petrella, R. J.; Roux, B.; Won, Y.; Archontis, G.; Bartels, C.; Boresch, S. CHARMM: the biomolecular simulation program. *Journal of Computational Chemistry* **2009**, *30* (10), 1545-1614.

51 Jorgensen, W. L.; Tirado-Rives, J. Potential energy functions for atomic-level simulations of water and organic and biomolecular systems. *Proceedings of the National Academy of Sciences* **2005**, *102* (19), 6665-6670.

52 Martyna, G. J.; Tobias, D. J.; Klein, M. L. Constant pressure molecular dynamics algorithms. *The Journal of Chemical Physics* **1994**, *101* (5), 4177-4189.

53 Essmann, U.; Perera, L.; Berkowitz, M. L.; Darden, T.; Lee, H.; Pedersen, L. G. A smooth particle mesh Ewald method. *The Journal of Chemical Physics* **1995**, *103* (19), 8577-8593.

จุฬาลงกรณ์มหาวิทยาลัย
Chulalongkorn University

จุฬาลงกรณ์มหาวิทยาลัย
Chulalongkorn University

VITA

NAME	Pisit Lettanakij
DATE OF BIRTH	15 October 1997
PLACE OF BIRTH	Bangkok, Thailand
INSTITUTIONS ATTENDED	B.Sc. in Chemistry (2019), Chulalongkorn University
HOME ADDRESS	19 Wararom village Bangbon 5 rd. Bangkok 10150
PUBLICATION	Pure and applied chemistry international conference 2023 (PACCON2023)

จุฬาลงกรณ์มหาวิทยาลัย
CHULALONGKORN UNIVERSITY